

# Hold Tight and Never Let Go: Security of Deep Learning based Automated Lane Centering under Physical-World Attack

Takami Sato\*  
University of California, Irvine  
takamis@uci.edu

Junjie Shen\*  
University of California, Irvine  
junjies1@uci.edu

Ningfei Wang  
University of California, Irvine  
ningfei.wang@uci.edu

Yunhan Jack Jia  
ByteDance AI Lab  
yunhan.jia@bytedance.com

Xue Lin  
Northeastern University  
xue.lin@northeastern.edu

Qi Alfred Chen  
University of California, Irvine  
alfchen@uci.edu

## ABSTRACT

Automated Lane Centering (ALC) systems are convenient and widely deployed today, but also highly security and safety critical. In this work, we are the first to systematically study the security of state-of-the-art deep learning based ALC systems in their designed operational domains under physical-world adversarial attacks. We formulate the problem with a safety-critical attack goal, and a novel and domain-specific attack vector: dirty road patches. To systematically generate the attack, we adopt an optimization-based approach and overcome domain-specific design challenges such as camera frame inter-dependencies due to dynamic vehicle actuation, and the lack of objective function design for lane detection models.

We evaluate our attack method on a production ALC system using 80 attack scenarios from real-world driving traces. The results show that our attack is highly effective with over 92% success rates and less than 0.95 sec average success time, which is substantially lower than the average driver reaction time. Such high attack effectiveness is also found (1) robust to motion model inaccuracies, different lane detection model designs, and physical-world factors, and (2) stealthy from the driver’s view. To concretely understand the end-to-end safety consequences, we further evaluate on concrete real-world attack scenarios using a production-grade simulator, and find that our attack can successfully cause the victim to hit the highway concrete barrier or a truck in the opposite direction with 98% and 100% success rates. We also discuss defense directions.

## 1 INTRODUCTION

Automated Lane Centering (ALC) is a Level-2 driving automation technology that automatically steers a vehicle to keep it centered in the traffic lane [1]. Due to its high convenience for human drivers, today it is widely available on various vehicle models such as Tesla, GM Cadillac, Honda Accord, Toyota RAV4, Volvo XC90, Nissan Rogue, Hyundai Sonata, etc. While convenient, such system is highly security and safety critical: When the ALC system starts to make wrong steering decisions, the human driver may not have enough reaction time to prevent safety hazards such as driving off road or colliding into vehicles in adjacent lanes, especially those in the opposite direction. Even with collision avoidance systems, it cannot prevent the vehicle from hitting the curb, falling down the highway cliff, or being hit by other vehicles that fail to yield. Thus, it is imperative and urgent to understand the security property of ALC systems.

To achieve its intelligent driving function, the most critical step in an ALC system is *lane detection*, which is naturally performed using cameras since lane lines are visual patterns. So far, Deep Neural Network (DNN) based lane detection achieves the highest accuracy [2] and is adopted in the most performant production ALC systems today such as Tesla Autopilot [3]. Thus, the end-to-end security of state-of-the-art ALC systems today highly depends on the security of such DNN-based lane detection models.

Recent works show that DNNs are vulnerable to physical-world adversarial attacks such as malicious stickers on traffic signs [4–7]. However, none of their methods can be directly applied to attack ALC systems due to 3 unique design challenges: (C1) There lacks a physical-world attack vector that can appear to be legitimately deployed around traffic lane areas. Existing ones such as small stickers are not ideal since directly performing them to traffic lanes is illegal [8]. (C2) In ALC systems, the physical-world attack generation needs to handle *inter-dependencies* among camera frames due to dynamic vehicle actuation. For example, if the attack deviates the detected lane to the right in a frame, the ALC system will steer the vehicle to the right accordingly. This causes the following frames to capture road areas more to the right, and thus directly affect their attack generation. To the best of our knowledge, no prior works consider such strong frame inter-dependencies in attack generation. (C3) The optimization objective function designs in prior works are mainly for image classification or object detection models and thus aim at changing class or bounding box probabilities [4, 7]. However, attacking lane detection requires to change the *shape* of the detected lane and thus none of these designs can directly apply.

The only prior effort that studied adversarial attacks on a production ALC system is from Tencent [9], which fooled the ALC system in Tesla Autopilot to follow fake lane lines created by white stickers on road regions originally *without lane lines*. However, it is neither attacking the designed operational domain for ALC systems, i.e., roads *with lane lines*, nor generating the perturbations systematically by addressing any of the 3 design challenges above.

To fill this critical research gap, in this work we are the first to systematically study the security of DNN-based ALC systems in their designed operational domains (i.e., roads with lane lines) under physical-world adversarial attacks. Since ALC systems assume a fully-attentive human driver prepared to take over at any time [1, 10], we identify the attack goal as not only causing the victim a lateral deviation (i.e., to the left or right) large enough to drive out of the current lane boundaries, but also achieving it shorter than the average driver reaction time to road hazard. This thus directly

\*Co-first authors

breaks the design goal of ALC systems and can cause various types of safety hazards such as driving off road and vehicle collisions.

Targeting this attack goal, we design a novel physical-world adversarial attack method on ALC systems, called *DRP (Dirty Road Patch) attack*, which is the first to systematically address all the 3 design challenges above. To address challenge C1, we are the first to identify *dirty road patches* as an attack vector in physical-world adversarial attacks. This design has 2 unique advantages: (1) Road patches can appear to be legitimately deployed on traffic lanes in the physical world, e.g., for fixing road cracks; and (2) Since it is common for real-world roads to have dirt or white stains, using similar dirty patterns as the input permutations can allow the malicious road patch to appear more normal and thus stealthier.

With this novel and domain-specific attack vector, we then design systematic malicious road patch generation following an optimization-based approach, which has shown both high efficiency and effectiveness in prior works [4, 11]. In this process, to efficiently and effectively address challenge C2 without heavyweight road testing or simulations, we design a novel method that combines vehicle motion model and perspective transformation to dynamically synthesize camera frame updates according to a lightweight simulated driving trajectory. It only needs one ALC system input trace on the target road without attack, which can be easily obtained.

Next, to address challenge C3, one direct solution is to design the objective function to directly change the steering angle decisions. However, we find that the lateral control step in ALC systems that calculates steering angle decisions are generally not differentiable, which makes it difficult to effectively optimize. To address this, we design a novel lane-bending objective function as a differentiable surrogate that is equivalent at lateral control design level. We also have other domain-specific designs in the optimization process, e.g., for attack robustness, stealthiness, and physical-world realizability.

We evaluate our attack method on a production ALC system in OpenPilot [12], which is reported to have state-of-the-art performance similar to Tesla Autopilot and GM Super Cruise, and better than all others [13–15]. We perform experiments on 80 attack scenarios from real-world driving traces, and find that our attack is highly effective with over 92% success rates for all scenarios, and less than 0.95 sec average success time, which is substantially lower than 2.5 sec, the average driver reaction time (§3.1). This means that even for a fully-attentive human driver who can take over as soon as the attack starts to take effect, her average reaction time is still far from enough to prevent the damage. We further find that such high effectiveness is robust to motion model inaccuracies and different lane detection model designs. We also find that the malicious dirty patterns appear smaller than, or at least similar, to real-world dirty patterns at 2.5 sec before the attack succeeds. However, if the human driver is not alerted and takes over at this point, s/he misses the last chance to prevent the damage (on average).

To understand the attack realizability in the physical world without incurring legal and safety concerns, we further design miniature-scale experiments, where the road and the malicious road patch are physically printed out on papers and set up in miniature scale. This allows us to evaluate our attack against 3 main physical-world factors: lighting condition, printer color accuracy, and camera sensing capability. Our results show that the physically-printed malicious

road patch causes the steering angle decision to change substantially from  $0.9^\circ$  to the right to  $22.3^\circ$  to the left, which demonstrates a high physical-world realizability of our attack.

To more concretely understand the end-to-end safety consequences of our attack, we further construct concrete real-world attack scenarios and perform attack evaluation using a production-grade simulator. The results show that our attack can successfully cause the victim to hit the highway concrete barrier or a truck in the opposite direction with 98% and 100% success rates respectively. The simulated attack consequences in both scenarios look quite dangerous and can be fatal, and also happen very fast within  $\sim 1$  second. Demo videos showing such end-to-end attack impact are available at: <https://sites.google.com/view/cav-sec/alc-adv-attack>.

Considering the popularity of ALC systems and the severe safety implications shown in this paper, the discovered attack requires community attention and defense discussion. Thus, we also discuss defense directions for DNN models and via sensor/data fusion.

In summary, this work makes the following contributions:

- We are the first to systematically study the security of DNN-based ALC systems in their designed operational domains under physical-world adversarial attacks. We formulate the problem with a safety-critical attack goal, and a novel and domain-specific attack vector, dirty road patches.
- To systematically generate malicious road patches, we adopt an optimization-based approach with 2 major novel and domain specific designs: motion model based input generation, and lane-bending objective function. We also have domain-specific designs for improving the malicious road patch robustness, stealthiness, and physical-world realizability.
- We evaluate our attack method on a production ALC system using 80 attack scenarios from real-world driving traces. The results show that our attack is highly effective with  $\geq 92\%$  success rates and  $\leq 0.95$  sec average success time, which is substantially lower than the average driver reaction time. Such high effectiveness is also found (1) robust to motion model inaccuracies, different lane detection model designs, and physical-world factors, and (2) stealthy from the driver’s view.
- To concretely understand the end-to-end safety consequences, we further evaluate on concrete real-world attack scenarios using a production-grade simulator. The results show that our attack can successfully cause the victim to hit the highway concrete barrier or a truck in the opposite direction with 98% and 100% success rates. We also discuss defense directions.

## 2 BACKGROUND

### 2.1 Overview of DNN-based ALC Systems

Fig. 1 shows an overview of a typical ALC system design [12, 16, 17], which operates in 3 steps to achieve automated lane centering:

**Lane Detection (LD).** Lane detection is the most critical step in an ALC system, since the driving decisions later are made solely based on its output. Camera is the most frequently used sensor for this step [18] since it is not only a natural choice as lane lines are visual patterns, but also cheap. On the camera frames, a Lane Detection (LD) model is used to detect lane lines. Recently, DNN-based LD models achieve the state-of-the-art accuracy [19–21] and thus are adopted in the most performant production ALC systems

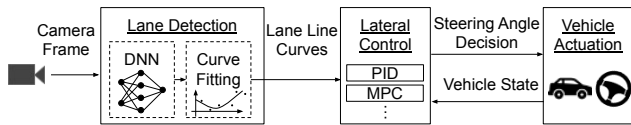


Figure 1: Overview of the typical ALC system design.

today such as Tesla Autopilot [3]. Since lane line shapes do not change much across consecutive frames, Recurrent Neural Network (RNN) is widely adopted in LD models to achieve more stable prediction [12, 22, 23]. LD models typically first predict the lane line points, and then post-process them to lane line curves for denoising and data compression, using curve fitting algorithms [19, 20, 24, 25].

Before the LD model is applied, a Region of Interest (ROI) filtering is usually performed to the raw camera frame to crop the most important area out of it (i.e., the road surface with lane lines) as the model input. Such ROI area is typically around the center and much smaller than the original frame, to improve the model performance and accuracy [26]. In §4.2, we leverage this in our design to achieve a lightweight synthesis of the attack-influenced camera frames.

**Lateral control.** This step calculates *steering angle decisions* to keep the vehicle driving at the center of the detected lane line curves. It first computes a desired driving path, which is typically at the center of the detected left and right lane lines [27]. Next, a control loop mechanism, e.g., Proportional-Integral-Derivative (PID) controller [28] or Model Predictive Control (MPC) [29], is applied to calculate the optimal steering angle decisions that can follow the desired driving path as much as possible considering the current vehicle state and physical constraints.

**Vehicle actuation.** This step interprets the steering angle decision into actuation commands, i.e., steering angles or torques. Here, the actuated steering changes are limited by a maximum value due to the physical constraints of the mechanical control units and also for driving stability and safety [27]. For example, in our experiments with a production-level ALC system with 100 Hz control frequency, such limit is  $0.25^\circ$  per control step (every 10 ms) for vehicle models such as Tesla Model S [30]. As detailed later in §3.3, such steering limit introduces a unique challenge to our design.

## 2.2 Physical-World Adversarial Attacks

Recent works find that DNN models are generally vulnerable to adversarial example, or adversarial attacks [11, 31]. Some works further explored such attacks in the physical world [5–7, 32–40], e.g., it is found that camera-based object detection models can be fooled by just adding small stickers to the Stop sign [5–7]. While these prior works concentrate on DNN models for image classification, object detection, and end-to-end autonomous driving tasks, we are the first to systematically study such attacks on production-level DNN-based ALC systems, which requires to address various new and unique design challenges as detailed later in §3.3.

## 3 ATTACK FORMULATION AND CHALLENGE

### 3.1 Attack Goal and Incentives

In this paper, we consider an attack goal that directly breaks the design goal of ALC systems: causing the victim vehicle a lateral deviation (i.e., deviating to the left or right) large enough to drive out of the current lane boundaries. Meanwhile, since ALC systems assume a fully-attentive human driver who is prepared to take

Table 1: Required deviations and success time for successful attacks on ALC systems on highway and local roads. Detailed calculations and explanations are in Appendix A.

Road Type	Required Lateral Deviation	Required Success Time
Highway	0.735 meters	<2.5 seconds (average driver reaction time to road hazard)
Local road	0.285 meters	

over at any moment [1, 10], such deviation needs to be achieved fast enough so that the human driver cannot react in time to take over and steer back. Table 1 shows concrete values of these two requirements for successful attacks on highway and local roads respectively, which will be used as evaluation metrics later in §5. In the table, the required deviations are calculated based on representative vehicle and lane widths in the U.S., and the required success time is determined using commonly-used average driver reaction time to road hazards, which is detailed in Appendix A. Specifically, we find multiple driver reaction time values referenced in different government-issued transportation policy guidelines [41–44], and we choose the *smallest* one (2.5 sec [41]) to avoid possible overestimation of the attack effectiveness in our evaluation.

**Safety implications.** The attack goal above can directly cause various types of safety hazards in the real world: (1) *Driving off road*, which is a direct violation of traffic rules [45] and can cause various safety hazards such as hitting road curbs or falling down the highway cliff. Note that these cannot be prevented even when the vehicle can perform perfect obstacle or collision avoidance. (2) *Vehicle collisions*, e.g., with vehicles parked on the road side, or driving in adjacent or opposite traffic lanes. Even when the vehicle can perform obstacle or collision avoidance, these collisions are still possible for two reasons. First, today’s obstacle and collision avoidance systems are not perfect. For example, a recent study shows that automatic braking systems in popular vehicle models today fail to avoid crashes 60% of the time [46]. Second, even if they can successfully perform emergency stop, they cannot prevent the victim from being hit by other vehicles that fail to yield on time, given the 2.5 sec average reaction time for human drivers. Later in §6, we construct end-to-end real-world attack scenarios to concretely evaluate and demonstrate these safety consequences.

**Attack incentives.** No matter whether the road accidents above are actually caused or not in the end, the victim vehicles under the attack goal are already exhibiting unsafe driving behaviors. These can thus already *damage the reputation* of the corresponding vehicle manufacturers or ALC system providers. Thus, a likely attack incentive can be *business competition*, which can allow one vehicle manufacturers or ALC system provider to deliberately damage the reputation of its rival companies and thus unfairly gain competitive advantages on the market. Meanwhile, considering the direct safety impact, we also cannot rule out the possible incentives for terrorist attacks, e.g., for political or financial purposes.

### 3.2 Threat Model

We assume that the attacker can obtain the same ALC system as the one used by the victim to get a full knowledge of its implementation details. This can be done through purchasing or renting the victim vehicle model and reverse engineering it, which has already been demonstrated possible on Tesla Autopilot [9]. Moreover, there exist production ALC systems that are directly open sourced [12]. We

also assume that the attacker can obtain a motion model [47] of the victim vehicle, which can be used to simulate its driving trajectory given the actuation commands, which will be used in our attack generation process (§4.2). This is a realistic assumption since the most widely-used motion model, which is also used by us in §4.2, only needs vehicle parameters such as steering ratio and wheelbase as input [47], which can be directly found from vehicle model specifications. We assume the victim drives at the speed limit of the target road, which is the most common case. In the attack preparation time, we assume that the attacker can collect the ALC system inputs (e.g., camera frames) of the target road by directly driving the victim vehicle model there with the ALC system on.

### 3.3 Design Challenges

As described in §2, DNN-based LD is the most critical step, and there are prior works that design successful physical-world adversarial attacks on DNN models. However, we find none of them can be directly applied to our problem due to 3 unique design challenges:

**C1. Lack of legitimately-deployable attack vector in the physical world.** To affect the camera input of an ALC system, it is ideal if the malicious perturbations can appear to be legitimately deployed around traffic lane regions in the physical world. To achieve high legitimacy, such perturbations also must not change the original human-perceived lane information. Prior works use small stickers or graffiti in physical-world adversarial attacks [4, 7, 9]. However, directly performing such activities to traffic lanes in public is illegal [8]. In our problem setting, the attacker needs to operate in the middle of the road when deploying the attack on traffic lanes. Thus, if the attack vector cannot be disguised as legitimate activities, it becomes highly difficult to deploy the attack in practice.

**C2. Need to handle camera frame inter-dependency due to dynamic vehicle actuation.** In real-world ALC systems, a successful attack on one single frame can barely cause any meaningful lateral deviations due to the steering actuation limit described in §2.1. For example, for the vehicle models with  $0.25^\circ$  limit in 10 ms and the camera frame rate is 20 Hz (a common one [12, 48]), each frame can at most introduce  $1.25^\circ$  steering angle changes, which can cause only *0.3-millimeter* lateral deviations at 45 mph.

Thus, to achieve our attack goal in §3.1, the attack must be continuously effective on a sequence of camera frames to increasingly reach larger actuated steering angles and thus larger lateral deviations per frame. In this process, due to the dynamic vehicle actuation applied by the ALC system, the attack effectiveness for later frames are directly dependent on that for earlier frames. For example, if the attack successfully deviates the detected lane to the right in a frame, the ALC system will steer the vehicle to the right accordingly. This causes the following frames to capture road areas more to the right, and thus directly affect their attack generation. Also, LD models typically use RNNs to improve prediction stability (§2.1), which thus further amplifies such inter-dependencies. There are prior works considering attack robustness across sequential frames, e.g., using EoT [34, 35], but none of them consider dynamic vehicle actuation and thus they still generate attacks without considering inter-dependencies across frames. However, as discussed above, for us it is necessary to handle them in the attack design.

**C3. Lack of differentiable objective function design for LD models.** To systematically generate adversarial inputs, prior works predominately adopt optimization-based approaches, which have shown both high efficiency and effectiveness [4, 11, 49, 50]. However, the objective function designs in these prior works are mainly for image classification [4, 35] or object detection [5–7] models, which thus aim at decreasing class or bounding box probabilities. However, as introduced in §2.1, LD models output detected lane line curves, and thus to achieve our attack goal the objective function design needs to aim at changing the *shape* of such curves. This is substantially different from decreasing probability values, and thus none of these existing designs can directly apply.

Closer to our problem, prior works that attack end-to-end autonomous driving models [37–40] directly design their objective function to change the final steering angle decisions. However, as described in §2.1, state-of-the-art LD models do not directly output steering angle decisions. Instead, they output lane line curves and rely on the lateral control step to compute the final steering angle decisions. However, many steps in the lateral control module, e.g., the desired driving patch calculation and the MPC framework, are generally not differentiable to the LD model input (i.e., camera frames), which makes it difficult to effectively optimize.

## 4 DIRTY ROAD PATCH ATTACK DESIGN

In this paper, we are the first to systematically address all the 3 design challenges in §3.3 by designing a novel physical-world attack method on ALC systems, called *Dirty Road Patch (DRP) attack*.

### 4.1 Design Overview

To address the 3 design challenges in §3.3, our DRP attack method has the following novel design components:

**Dirty road patch: Legitimately-deployable and stealthy physical-world attack vector.** To address challenge C1, we are the first to identify *dirty road patch* as an attack vector in physical-world adversarial attacks. This design has 2 unique advantages. First, road patches can appear to be legitimately deployed on traffic lanes in the physical world, e.g., for fixing road cracks. Today, deploying them is made easy with adhesive designs [51] as shown in Fig. 2. The attacker can thus take time to prepare the attack in house by carefully printing the malicious input perturbations on top of such adhesive road patches, and then pretend to be road workers like those in Fig. 2 to quickly deploy it when the target road is the most vacant, e.g., in late night, to avoid drawing too much attention.

Second, since it is common for real-world roads to have dirt or white stains such as those in Fig. 2, using similar dirty patterns as the input perturbations can allow the malicious road patch to appear more normal and thus stealthier. To mimic the normal dirty patterns, our design only allows color perturbations on the gray scale, i.e., black-and-white. To avoid changing the lane information as discussed in §3.3, in our design we (1) require the original lane lines to appear exactly the same way on the malicious patch, if covered by the patch, and (2) restrict the brightness of the perturbations to be strictly lower than that of the original lane lines. To further improve stealthiness, we also design parameters to adjust the perturbation size and pattern, which are more detailed in §4.3.3.





**Figure 2: Illustration of our novel and domain-specific attack vector: dirty road patch.**

**Motion model based input generation.** To address the strong inter-dependencies among the camera frames (challenge C2), we need to dynamically update the content of later camera frames according to the actuation decisions applied at earlier ones in the attack generation process. Since adversarial attack generation typically takes thousands of optimization iterations [52, 53], it is practically highly difficult, if not impossible, to drive real vehicles on the target road to obtain such dynamic frame update every time the perturbations are updated in an iteration. Another idea is to use vehicle simulators [54, 55], but it requires the attacker to first create a high-definition 3D scene of the target road in the real world, which requires a significant amount of hardware resource and engineering efforts. Also, launching a vehicle simulator in each optimization iteration can greatly harm the attack generation speed.

To efficiently and effectively address this challenge, we combine *vehicle motion model* [47] and *perspective transformation* [56, 57] to dynamically synthesize camera frame updates according to a driving trajectory simulated in a lightweight way. This method is inspired by Google Street View [58] that synthesizes 360° views from a limited number of photos utilizing perspective transformation. Our method only requires one trace of the ALC system inputs (e.g., camera frames) from the target road without attack, which can be easily obtained by the attacker (§3.2).

**Optimization-based dirty patch generation.** To systematically generate effective malicious patches, we adopt an optimization-based approach similar to prior works [4, 11]. To address challenge C3, we design a novel lane-bending objective function as a differentiable surrogate that aims at changing the derivatives of the desired driving path before the lateral control module, which is equivalent to change the steering angle decisions at the lateral control design level. Besides this, we also have other domain-specific designs in the optimization problem formulation, e.g., for a differentiable construction of the curve fitting process, malicious road patch robustness, stealthiness, and physical-world realizability.

Fig. 3 shows an overview of the malicious road patch generation process, which is detailed in the following sections.

## 4.2 Motion Model based Input Generation

In Fig. 3, step ①–⑦ belong to the motion model based input generation component. As described earlier in §4.1, the input to this component is a trace of ALC system inputs such as camera frames from driving on the target road without attack. In ①, we apply *perspective transformation*, a widely-used computer vision technique that can project an image view from a 3D coordinate system to a 2D plane [56, 57]. Specifically, we apply it to the original camera

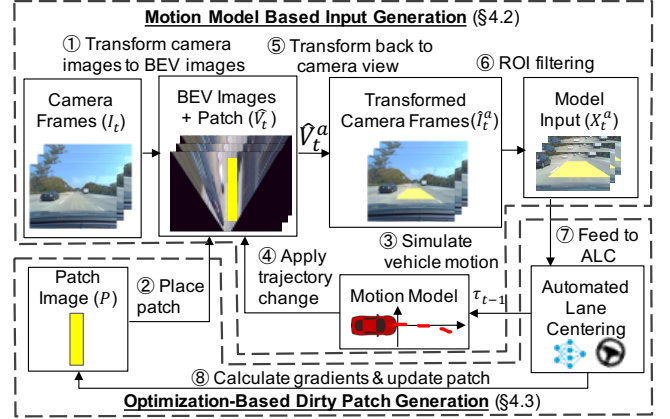


**Figure 3: Overview of our DRP (Dirty Road Patch) attack method. ROI: Region of Interest; BEV: Bird’s Eye View.**

frames from the driver’s view to obtain their Bird’s Eye View (BEV) images. This transformation is highly beneficial since it makes our later patch placement and attack-influenced camera frame updates much more natural and thus convenient. We denote this process as  $V_t := \text{BEV}(I_t)$ , where  $I_t$  and  $V_t$  are the original camera input and its BEV view respectively at frame  $t$ . This process is invertible, i.e., we can also obtain  $I_t$  with  $\text{BEV}^{-1}(V_t)$ .

Next, in ②, we obtain the generated malicious road patch image  $P$  from the optimization-based dirty patch generation component (§4.3) and place it on  $V_t$  to obtain the BEV image with the patch, denoted as  $\widehat{V}_t := \Lambda(V_t, P)$ . To achieve consistent road patch placements in the world coordinate across frames, we calculate the *pixel-meter relationship*, i.e., the number of pixels per meter, in the BEV images based on the driving trace of the target road. With this, we can place the patch in each frame precisely based on the driving trajectory changes across frames.

Next, we compute the vehicle moving trajectory changes caused by the placed malicious road patch, and reflect such changes in the camera frames. We represent the vehicle moving trajectory as a sequence of vehicle states  $S_t := [x_t, y_t, \beta_t, v_t]$ , ( $t = 1, \dots, T$ ), where  $x_t, y_t, \beta_t, v_t$  are the vehicle’s 2D position, heading angle, and speed at frame  $t$ , and  $T$  is the total number of frames in the driving trace. Thus, the trajectory change at frame  $t$  is  $\delta_t := S_t^a - S_t^o$ , where  $S_t^a$  and  $S_t^o$  are vehicle states with and without attack respectively.

To calculate  $\delta_t$  caused by the attack effect at the frame  $t - 1$ , we need to know the attack-influenced vehicle state  $S_t^a$ . To achieve that, we use a *vehicle motion model* to simulate the vehicle state  $S_t^a$  by feeding the steering angle decision  $\tau_{t-1}$  from the lateral control step in the ALC system (§2.1) given the attacked frame at  $t - 1$  and the previous vehicle state  $S_{t-1}^a$ , denoted as  $S_t^a := \text{MM}(S_{t-1}^a, \tau_{t-1})$ . A vehicle motion model is a set of parameterized mathematical equations representing the vehicle dynamics and can be used to simulate its driving trajectory given the speed and actuation commands. In this process, we set the vehicle speed as the speed limit of the target road as described in our threat model (§3.2). In our design, we adopt the kinematic bicycle model [59], which is the most widely-used motion model for vehicles [59–61].

With  $\delta_t$ , in ④ we then apply affine transformations on the BEV image  $\widehat{V}_t$  to obtain the attack-influenced one  $\widehat{V}_t^a$ , denoted as  $\widehat{V}_t^a := T(\widehat{V}_t, \delta_t)$ . Fig. 4 shows an example of the shifting and rotation  $T(\cdot)$

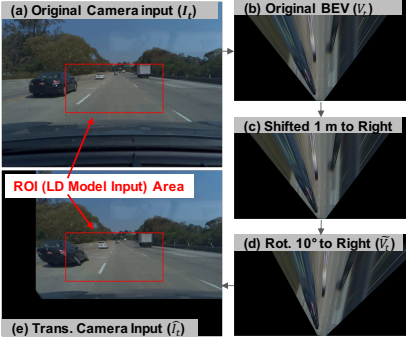


Figure 4: Motion model based input generation from original camera input.

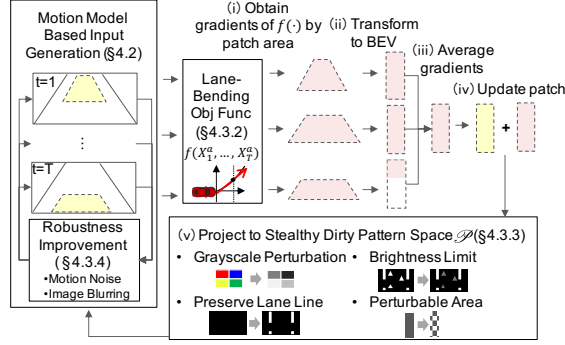


Figure 5: Iterative optimization process design for our optimization-based dirty patch generation.

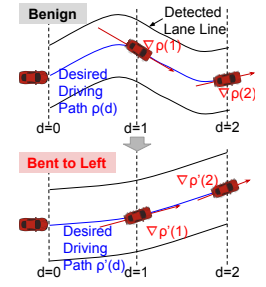


Figure 6: “Lane bending” effect of our objective function by maximizing  $\nabla\rho(d)$  at each curve point.

in the BEV, which synthesizes a camera frame with the vehicle position shifted by 1 meter and rotated by  $10^\circ$  to the right. Although it causes some distortion and missing areas on the edge, the ROI area (red rectangle), i.e., the LD model input, is still complete and thus sufficient for our purpose. Since the ROI area is typically focused on the center and much smaller than the raw camera frame (§2.1), our method can successfully synthesize multiple complete attack-influenced LD model inputs from only 1 ALC system input trace.

Next, in ⑤, we obtain the attack-influenced camera frame at the driver’s view  $\hat{I}_t^a$ , i.e., the direct input to the ALC system, by projecting  $\hat{V}_t^a$  back using  $\hat{I}_t^a := \text{BEV}^{-1}(\hat{V}_t^a)$ . Next, in ⑥, the ROI filtering from the ALC system is used to extract the model input  $X_t^a := \text{ROI}(\hat{I}_t^a)$ .  $X_t^a$  and vehicle state  $S_t^a$  are then fed to the ALC system in ⑦ to obtain the steering angle decision  $\tau_t$ , denoted as  $\tau_t := \text{ALC}(X_t^a, S_t^a)$ . Step ③–⑦ are then iteratively applied to obtain  $\hat{I}_{t+1}^a, \hat{I}_{t+2}^a, \dots$  one after one until all the original frames are updated to reflect the moving trajectory changes caused by  $P$ . These updated attack-influenced inputs are then fed to the optimization-based dirty patch generation component, which is detailed next.

### 4.3 Optimization-based Dirty Patch Generation

In Fig. 3, step ⑧ belongs to the optimization-based road path generation component. In this step, we design a domain-specific optimization process on the target ALC system to systematically generate the malicious dirty road patch  $P$ .

**DRP attack optimization problem formulation.** We formulate the attack generation as the following optimization problem:

$$\min \mathcal{L} \quad (1)$$

$$\text{s.t. } X_t^a = \text{ROI}(\text{BEV}^{-1}(T(\Lambda(V_t, P), S_t^a - S_t^o))) \quad (t = 1, \dots, T) \quad (2)$$

$$\tau_t^a = \text{ALC}(X_t^a, S_t^a) \quad (t = 1, \dots, T) \quad (3)$$

$$S_{t+1}^a = \text{MM}(S_t^a, \tau_t^a) + \epsilon_t \quad (t = 1, \dots, T-1) \quad (4)$$

$$S_1^a = S_1^o \quad (5)$$

$$P = \text{BLUR}(\text{FILL}(B) + \Delta) \quad (6)$$

$$\Delta \in \mathcal{P} \quad (7)$$

where the  $\mathcal{L}$  in Eq. 1 is an objective function that aims at deviating the victim out of the current lane boundaries as soon as possible by minimizing it, which is detailed in §4.3.2. Eq. 2–5 have been described in §4.2. In Eq. 6, the patch image  $P \in \mathbb{R}^{H \times W \times C}$  consists of a base color  $B \in \mathbb{R}^C$  and the perturbation  $\Delta \in \mathbb{R}^{H \times W \times C}$ , where  $W, H$ , and  $C$  are the patch image width, height, and the number

of color channels respectively. We select an asphalt-like color as the base color  $B$  since the image is designed to mimic a road patch. Function  $\text{FILL}: \mathbb{R}^C \rightarrow \mathbb{R}^{H \times W \times C}$  fills  $B$  to the entire patch image. Since we aim at generating perturbations that mimic the normal dirty patterns on roads, we restrict  $\Delta$  to be within a stealthy road pattern space  $\mathcal{P}$ , which is detailed in §4.3.3. We also include a noise term  $\epsilon_t$  in Eq. 4 and a image blurring function  $\text{BLUR}(\cdot)$  in Eq. 6 to improve the patch robustness to vehicle motion model inaccuracies and camera image blurring, which are detailed in §4.3.4 and §4.3.5.

**4.3.1 Optimization Process Overview.** Fig. 5 shows an overview of our iterative optimization process design to solve the optimization problem above. Given an initial patch image  $P$ , we obtain the model input  $X_1^a, \dots, X_T^a$  from the motion model based input generation process. In step (i), we calculate the gradients of the objective function with respect to  $X_1^a, \dots, X_T^a$ , and only keep the gradients corresponding to the patch areas. In step (ii), these gradients are projected into the BEV space. In step (iii), we calculate the average BEV-space gradients weighted by their corresponding patch area sizes in the model inputs. This weighted averaging is designed to prevent the averaged gradient from being dominated by the earlier frames, where the patch is far and small but the whole patch is visible. Next, in step (iv), we update the current patch with Adam [62] using the averaged gradient as the gradient of the patch image. In step (v), we then project the updated patch into the stealthy road pattern space  $\mathcal{P}$ . This updated patch image is then fed back to the motion model based input generation module, where we also add robustness improvement such as motion noises and image blurring. We terminate this optimization process when the attack-introduced lateral deviations obtained from the motion model are large enough.

**4.3.2 Lane-Bending Objective Function Design.** As discussed in §4.1, directly using steering angle decisions as  $\mathcal{L}$  makes the objective function non-differentiable to  $X_1^a, \dots, X_T^a$ . To address this, we design a novel lane-bending objective function  $f(\cdot)$  as a differentiable surrogate function. In this design, our key insight is that at the design level, the lateral control step aims at making steering angle decisions that follows a *desired driving path* in the middle of the detected left and right lane line curves from the lane detection step (§2.1). Thus, changing the steering angle decisions is equivalent to changing the derivatives of (or “bending”) such desired driving path curve. This allows us to design  $f(\cdot)$  as follows:

$$f(X_1^a, \dots, X_T^a) = \sum_{t=1}^T \sum_{d \in D_t} \nabla \rho_t(d; \{X_j^a | j \leq t\}, \theta) + \lambda \|\Omega_t(X_T^a)\|_p \quad (8)$$

where  $\rho_t(d)$  is a parametric curve whose parameters are decided by (1) both the current and previous model inputs  $\{X_j^a | j \leq t\}$  due to frame inter-dependencies (§3.3), and (2) the LD model DNN parameters  $\theta$ .  $D_t$  is a set of curve point index  $d = 0, 1, 2, \dots$  for the desired driving path curve at frame  $t$ .  $\lambda$  is the weight of the  $p$ -norm regularization term, which is designed for stealthiness and detailed later in §4.3.3. We then can define  $\mathcal{L}$  in Eq. 1 as  $f(\cdot)$  and  $-f(\cdot)$  when attacking to the left and right respectively. Fig. 6 illustrates this surrogate function design when attacking to the left. As shown, by maximizing  $\nabla \rho_t(d)$  at each curve point in Eq. 8, we can achieve a “lane bending” effect to the desired driving path curve. Since the direct LD model output is lane line points (§2.1) but  $\rho_t(\cdot)$  require lane line curves, we further perform a *differentiable construction of the curve fitting process*, which is detailed in Appendix B.

**4.3.3 Designs for Dirty Patch Stealthiness.** As described in §4.1, we design the perturbations on the malicious road patch to mimic real-world dirty patterns such as those in Fig. 2 so that they can appear more normal and thus stealthier. Specifically, 4 stealthiness designs are considered in the stealthy road pattern space  $\mathcal{P}$  in the optimization process (Eq. 7) as follows:

**Grayscale perturbation.** Real-world dirty patterns on the road are usually created by dust or white stains (Fig. 2), and thus most commonly just appear white. Thus, we cannot directly follow previous works in the image space [7] to allow perturbations with arbitrary colors. Thus, our design restricts our perturbation  $\Delta$  in the grayscale (i.e., black-and-white). To achieve this, we perturb  $\Delta$  in the YCbCr color space [63] instead of the RGB space, by only allowing to increase its Y channel (the grayscale channel) value, denoted as  $\Delta_Y \geq 0$ , with its Cb and Cr channel values always zero.

**Preserving original lane line information.** We preserve the original lane line information by drawing the same lane lines as the original ones on the patch (if covered by the patch). Note that without this our attack can be easier to succeed, but as discussed in §3.3, it is much more preferred to preserve such information so that the attack deployment process can more easily appear as legitimate road work activities and the deployed patch is less likely to be legitimately removed due to the lack of the correct lane lines.

**Brightness limits.** While the dirty patterns are restricted to grayscale, they are still the darker, the stealthier. Also, to best preserve the original lane information, the brightness of the dirty patterns should not be more than that of the original lane lines. Thus, we (1) add the  $p$ -norm regularization term in the objective function (Eq. 8) to suppress the amount of  $\Delta_Y$ , and (2) restrict  $B_Y + \Delta_Y < \text{LaneLine}_Y$ , where  $B_Y$  and  $\text{LaneLine}_Y$  are the Y channel values for the base color and original lane line color respectively.

**Perturbation area restriction.** Besides brightness, also the fewer patch areas are perturbed, the stealthier. Thus, we define Perturbable Area Ratio (PAR) as the percentage of pixels on  $P$  that can be perturbed in the optimization process. Thus, when PAR=30%, 70% pixels on  $P$  will only have the base color  $B$ .

**4.3.4 Dirty Patch Robustness Improvement.** In our attack generation process, we use the vehicle moving trajectory simulated by a

motion model to judge the attack effectiveness (§4.3.1). However, all motion models have inaccuracies due to the difficulty in precisely modeling all the complex and dynamic interactions among the road, tires, and the vehicle internal components in the real world. Thus, when the generated road patch is deployed in practice, the actual moving behaviors of the victim will be different from the simulated ones by our motion model in the attack generation time. Thus, to improve the attack robustness, we add noises  $\epsilon_t$  to the vehicle state  $S_t^a$  during the motion model based input generation process. More specifically, we apply  $\epsilon_t$  following a normal distribution  $\mathcal{N}(0, \alpha)$  to both of the  $MM(\cdot)$  outputs that are used in our input generation: the lateral position  $y_t$ , and the heading angle  $\beta_t$ .

**4.3.5 Designs for Physical-World Realizability.** After the malicious road patch is generated digitally, the color and pattern of its perturbations can be perceived differently by camera devices in the physical world due to 3 main practical factors: (1) the lighting condition, (2) printer color accuracy, and (3) camera sensing capability, e.g., color accuracy and image clarity. Such differences can thus degrade the attack effectiveness when applying our attack in practice.

To address this, we create a color mapping between the intended colors and the camera-perceived colors after the intended ones are physically printed and captured by the camera device of the targeted ALC system. In our attack context, the attacker can do the same on the target road. Since our malicious road patches are designed to be only in grayscale for stealthiness (§4.3.3), we constrain the color mapping in the gray scale instead of full color. Then after the patch is generated digitally, we perform a post-processing step that uses the color mapping to transform the color of each pixel to the color that can be mapped to the intended one after being printed. In addition, we apply the Gaussian blur to both the patch and gradients during the optimization process to address potential image blurring introduced by the camera.

## 5 ATTACK METHODOLOGY EVALUATION

In this section, we evaluate the effectiveness, robustness, generality, and realizability of our DRP attack methodology.

**Targeted ALC system.** In our evaluation, we perform experiments on the production ALC system in OpenPilot [12], which follows the state-of-the-art DNN-based ALC system design (§2.1). OpenPilot is an open-source production Level-2 driving automation system that can be easily installed in over 80 popular vehicle models (e.g., Toyota, Chrysler, Cadillac, etc.) by mounting a dashcam. We select OpenPilot due to its (1) *representativeness*, since it is reported to have state-of-the-art performance similar to Tesla Autopilot and GM Super Cruise and better than all other manufacturers [13–15], (2) *practicality*, from the large quantity and diversity of vehicle models it can support [12], and (3) *ease to experiment with*, since it is the only production ALC system that is open sourced. In this paper, we mainly evaluate on the lane detection model in OpenPilot v0.7.0, which is released in Dec. 2019. In our methodology generality evaluation in §5.3, we also experiment on LD models from older OpenPilot versions that have different DNN designs.

**Evaluation dataset.** In this section, we perform experiments using the comma2k19 dataset [64], which contains over 33 hours driving traces between California’s San Jose and San Francisco in a Toyota RAV4 2017 driven by human drivers. These traces are

collected using the official OpenPilot dashcam device, called EON, which is thus directly compatible with OpenPilot. These traces include not only the road-facing camera frames, but also the vehicle steering angle, speed, position, and heading angle associated with each frame, which are used as inputs to our motion model based input generation module (§4.2).

From this dataset, we manually look for short driving periods with a clear driving path ahead, e.g., no front vehicles, to make road patch placement convenient. In total, we obtain 40 eligible short driving clips, 10 seconds each, with half of them on the highway, and half on local roads. For each driving clip, we consider two attack scenarios: attack to the left, and to the right. Thus, in total we evaluate 80 different attack scenarios.

## 5.1 Attack Effectiveness

**Evaluation methodology and metrics.** We evaluate the attack methodology effectiveness using the evaluation dataset described above. For each attack scenario, we use our DRP attack method to generate a road patch, and use the motion model based input generation method in §4.2 to simulate the vehicle driving trajectory influenced by the malicious road patch. To judge the attack success, we use the attack goal defined in §3.1 and concrete metrics listed in Table 1, i.e., achieving over 0.735 meters and 0.285 meters lateral deviations on highway and local-road scenarios respectively within 2.5 seconds, the average driver reaction time to road hazards. We measure the achieved deviation by calculating the lateral distances at each time point between the vehicle trajectories with and without the malicious road patch, and use the earliest time point to reach the required deviation to calculate the success time.

Since ALC systems assume a human driver who is prepared to take over, it is better if the malicious road patch can also look stealthy enough at 2.5 seconds (driver reaction time) before the attack succeeds so that the driver won’t be alerted by its looking and decide to take over. Thus, in this section, we also study the stealthiness of the generated road patches. More specifically, we quantify their perturbation degrees using the average pixel value changes to the road patch base color in  $\mathcal{L}_1$ ,  $\mathcal{L}_2$  and  $\mathcal{L}_{inf}$  distances, the three common perturbation metrics used in adversarial machine learning research [65, 66]. Since the perturbation is constrained to positive (§4.3.3), in our context  $\mathcal{L}_1$  and  $\mathcal{L}_2$  mean how much brighter on average the perturbations are than the base color measured by absolute and Euclidean distances of pixel values respectively; and  $\mathcal{L}_{inf}$  means the largest brightness change to the base color among all pixels. In our evaluation, the pixel distances are measured in the RGB space and normalized to  $[0, 1]$ .

**Experimental setup.** For each scenario in the evaluation dataset, we manually mark the road patch placement area in the BEV view of each camera frame based on the lane width and shape. To achieve consistent road patch placements in the world coordinate across a sequence of frames, we calculate the number of pixels per meter in the BEV images and adjust the patch position in each frame precisely based on the driving trajectory changes across consecutive frames. The road patch sizes we use are 3.6–5.4 meters wide to accommodate the wider lanes on the highway, and 24–36 meters long to ensure at least a few seconds of visible time at high speed. The patches are placed 7 meters far from the victim at the starting

frame. For stealthiness levels, we evaluate the  $\mathcal{L}_2$  regularisation coefficient  $\lambda = 10^{-2}$ ,  $10^{-3}$ , and  $10^{-4}$ , with PAR set to 50%. According to Eq. 8, larger  $\lambda$  value means more suppression of the perturbation, and thus should lead to a higher stealthiness level. We mainly vary  $\lambda$  in this section since we found that the control of the perturbation degrees is dominated by  $\lambda$  when PAR is in a wide range around 50%. For the motion model, we directly use the vehicle parameters of Toyota RAV4 2017, the vehicle model that collects the driving traces in our dataset, to ensure the consistency. Specifically, the wheelbase is set to 2.65 meters, and  $l_f = l_r = 1.325$  meters.

**Results.** Table 2 shows the evaluation results. As shown, our attack is highly effective under all the 3 stealthiness levels: the success rates are 100% for all scenarios when  $\lambda = 10^{-4}$  and  $10^{-3}$ , and are only slightly lower, but still over 92%, for the highway scenarios when  $\lambda = 10^{-2}$ , the highest stealthiness level in our experiment. Such slight success rate decrease is due to the more constrained attack capability in adding perturbations when the stealthiness level increases. As will be discussed later, these stealthiness levels well correlate with the driver-perceived perturbation degrees, and when  $\lambda = 10^{-2}$ , the malicious dirty patterns on the road patch are almost invisible in the driver’s view at 2.5 sec (the average driver reaction time) before the attack succeeds. Among the successful cases, the average success time is all under 0.95 sec, which is substantially lower than 2.5 sec, the required success time. This means that even for a fully attentive human driver who is always able to take over as soon as the attack starts to take effect, her average reaction time is still far from enough to prevent the damage.

**Stealthiness.** As shown in Table 2, the  $\mathcal{L}_1$  and  $\mathcal{L}_2$  pixel distances decrease proportionally in substantial amount when  $\lambda$  increases, which means the average brightness of the perturbations is well-controlled by the  $\mathcal{L}_2$  regularization coefficient  $\lambda$ . In particular, the  $\mathcal{L}_1$  and  $\mathcal{L}_2$  distances are at most 0.074 and 0.114 respectively, which means that the perturbations are on average only 11.4% brighter than the base color even at the lowest stealthiness level in our experiment.  $\mathcal{L}_{inf}$  is always 0.201 for highway scenarios and 0.210 for local road scenarios, which means that the perturbations are at most 21% brighter than the base color.

To visually understand these stealthiness levels, Fig. 7 (a) shows the malicious road patch appearances at different stealthiness levels from the driver’s view at 2.5 seconds before our attack succeeds. As shown, in local road scenarios, some white dirty patterns can be seen on the road patches with the lowest stealthiness level ( $\lambda = 10^{-4}$ ), while the perturbations on the ones with the highest stealthiness level ( $\lambda = 10^{-2}$ ) are almost invisible. As shown, even for the lowest stealthiness level ( $\lambda = 10^{-4}$ ) in our experiment, the perturbations are still smaller than some real-world dirty patterns such as the left one in Fig. 7 (b). In addition, we find that the perturbations for all these 3 stealthiness levels are already much less intrusive than those in previous physical-world adversarial machine learning attacks in the image space, for example the state-of-the-art ones for traffic sign recognition [7] shown in Fig. 7 (c). In highway scenarios, since the speed is higher, the malicious road patches appear much farther away at 2.5 seconds before our attack succeeds compared to local road scenarios, which thus allows our attack to appear even stealthier as shown in the rightmost figure in Fig. 7 (a).

**Table 2: Attack success rate and time under different stealthiness levels. Larger  $\lambda$  means stealthier. Average success time is calculated only among the successful cases. Pixel  $\mathcal{L}_1$ ,  $\mathcal{L}_2$ , and  $\mathcal{L}_{inf}$  are the average pixel value changes to the road patch base color in the RGB space and normalized to  $[0, 1]$ .**

Stealthiness Level	Scenario Type	Succ. Rate	Ave. Succ. Time (sec)	Pixel $\mathcal{L}_1$	Pixel $\mathcal{L}_2$	Pixel $\mathcal{L}_{inf}$
$\lambda = 10^{-2}$	Highway	92.5%	0.901	0.014	0.038	0.201
	Local	100%	0.945	0.015	0.043	0.210
$\lambda = 10^{-3}$	Highway	100%	0.865	0.036	0.069	0.201
	Local	100%	0.926	0.037	0.073	0.210
$\lambda = 10^{-4}$	Highway	100%	0.854	0.069	0.107	0.201
	Local	100%	0.919	0.074	0.114	0.210

From Fig. 7 and Table 2, we find that the stealthiness level with  $\lambda = 10^{-3}$  strikes an ideal balance between attack effectiveness and stealthiness: it not only has similar or smaller white dirty patterns compared to real-world ones such as those shown in Fig. 7 (b) at 2.5 seconds before our attack succeeds, but also has no sacrifice of attack effectiveness as shown in Table 2. Thus, we use it as the default stealthiness configuration in our following experiments.

## 5.2 Robustness to Motion Model Inaccuracies

In this section, we evaluate the attack robustness to different levels of such inaccuracies. We first obtain the errors of the motion model used in our attack as 0.008 m mean with 0.002 m standard deviation based on previous measurement studies of motion models [59]. Next, we evaluate the attack with such errors randomly sampled from the uniform distribution  $U(-\Delta, \Delta)$  with different  $\Delta$  levels and added to both longitudinal and lateral directions independently at each control step. Our results shows that our attack maintains a high effectiveness with  $\geq 97.5\%$  success rates even when  $\Delta$  is 0.048 m (i.e.,  $8\times$  standard deviations, holds for a probability of  $1 - 10^{-13}$  in practice). More details are in Appendix C due to page limit.

## 5.3 Attack Generality Evaluation

To achieve end-to-end attack impact on ALC systems, our attack method is designed around exploiting the LD model, the most critical element in ALC systems (§2). Thus, in this section we evaluate the generality of our attack against LD models of different designs. Ideally we hope to evaluate on LD models from other production ALC systems besides OpenPilot, e.g., from Tesla Autopilot. However, to best of our knowledge, OpenPilot is the only one that is currently open sourced. Fortunately, we find that the LD models in some older versions of OpenPilot actually have different DNN designs (detailed below), which thus can also serve for our purpose.

**Experimental setup.** We select LD models from OpenPilot v0.7.0 (used in previous sections), v0.6.6, and v0.5.9 to perform this evaluation considering their large DNN architecture differences with each other, which are summarized in Table 3. Specifically, their numbers of trainable parameters and layers are quite different, e.g., the v0.5.9 model has 58-63% fewer weights and 58-60% fewer layers than the other two. At the DNN design level, they mainly differ by the use of naive RNN layers or a more advanced one called Gated Recurrent Unit (GRU), and whether to use Batch Normalization (BN) layers. More details are in Appendix D. The evaluation dataset and metrics are the same as §5.1. The experiments use  $\lambda = 10^{-3}$  and PAR=50%, the default stealthiness level as discussed in §5.1.

**Table 3: Evaluation results for attack generality against LD (Lane Detection) models of different DNN designs in OpenPilot. Evaluation metrics are the same as those in Table 2.**

LD Model	DNN Arch.	Scenario Type	Succ. Rate	Succ. Time (s)	Pixel $\mathcal{L}_1$	Pixel $\mathcal{L}_2$	Pixel $\mathcal{L}_{inf}$
v0.7.0	CNN+	Highway	100%	0.865	0.036	0.069	0.201
	GRU	Local	100%	0.926	0.037	0.073	0.210
v0.6.6	CNN+	Highway	90%	0.931	0.032	0.064	0.201
	BN+GRU	Local	95%	0.955	0.032	0.067	0.210
v0.5.9	CNN+	Highway	100%	0.891	0.039	0.076	0.201
	naive RNN	Local	100%	0.948	0.039	0.078	0.210

**Results.** Table 3 shows the results. As shown, our attack is able to achieve at least 90% and 95% success rates for the highway and local road scenarios respectively against all three LD models of different DNN designs, which shows a high generality of the attack methodology. Among them, the v0.6.6 model seems to have the highest robustness against our attack, with 5-10% lower success rates and also higher success time than those for the other models. Also, the  $\mathcal{L}_1$  and  $\mathcal{L}_2$  pixel distances for it are the smallest. Since its major design-level difference to the v0.7.0 model is BN layers, we suspect that such robustness increase might come from the use of BN layers. Interestingly, this is contradicting to latest researches that find BN layers can harm DNN model robustness [67]. We plan to systematically investigate this in the future. Between the v0.7.0 and v0.5.9 models, the attack effectiveness is very close. Thus, even though GRU is supposed to be more advanced and make the driving more stable, it does not show increased robustness to our attack.

## 5.4 Physical-World Realizability Evaluation

While we have shown high attack effectiveness, robustness, and generality on real-world driving traces in the sections above, the experiments are performed by synthesizing the patch placement and appearances digitally, which is thus still different from actually performing the attack in the physical world. As discussed in §4.3.5, there are 3 main practical factors that can affect the attack effectiveness in physical world: (1) the lighting condition, (2) printer color accuracy, and (3) camera sensing capability. Thus, in this section we perform experiments to understand the physical-world attack realizability against these 3 main practical factors.

**Evaluation methodology: miniature-scale experiments.** To perform the DRP attack, a real-world attacker can pretend to be road workers and place the malicious road patch on public roads. However, it is both unethical and illegal [8] for us as researchers to do so. It is also unsafe for us since ALC systems typically only operate when the speed is sufficiently high, e.g., 28 mph [12, 68]. Nevertheless, we still try our best to perform such evaluation by designing a *miniature-scale experiment*, where the road and the malicious road patch are first physically printed out on papers and placed according to the physical-world attack settings but in miniature scale. Then the real ALC system camera device are used to get camera inputs from such a miniature-scale physical-world setting. Such miniature-scale evaluation methodology can capture all the 3 main practical factors in the physical-world attack setting, and thus can sufficiently serve for the purpose of this evaluation.

**Experimental setup.** As shown in Fig. 10, we create a miniature-scale road by printing a real-world high-resolution BEV road texture on multiple ledger-size papers and concatenating them together to form a long straight road. In the attack evaluation time, we create



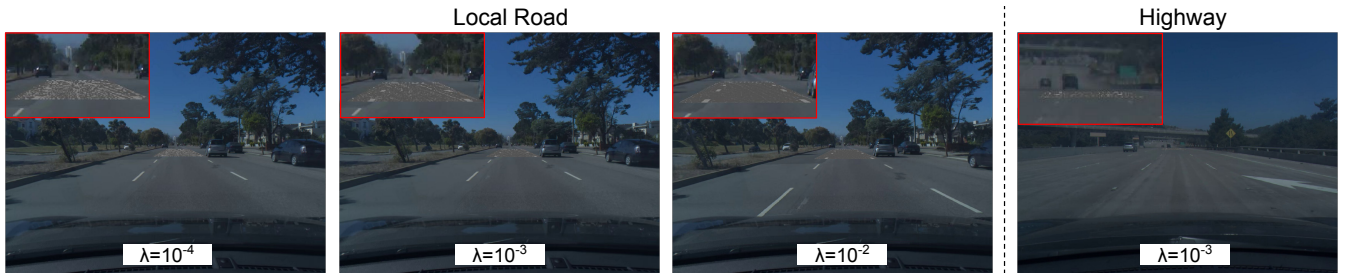


Figure 7: Driver’s view at 2.5 seconds (average driver reaction time to road hazards [41]) before our attack succeeds under different stealthiness levels. Inset figures are the zoomed-in views of the malicious road patches. Larger images are in Fig. 15.



Figure 8: Real-world dirty road patterns similar to our attack. Figure 9: Stop sign hiding and appearing attacks [7].

the miniature-scale malicious road patch using the same method, and place it on top of the miniature-scale road following our DRP attack design. We mount EON, the official OpenPilot dashcam device, on a tripod and face it to the miniature-scale road. The road size, road patch size, and the EON mounting position are carefully calculated to represent OpenPilot installed on a Toyota RAV4 driving on a standard 3.6-meter wide highway road at 1:12 scale. We also use two studio lights to imitate the daytime lighting condition.

As shown, the road texture image we select is a lane image with solid lane line on the left and a dotted lane line on the right, which is the most common lane marking setup for the leftmost lane in one driving direction. Thus, we set the attack goal in our experiments as to deviate the victim out of the lane on the left to hit the road barrier or crash into vehicles driving in the opposite direction (both have end-to-end attack consequence demonstrations later in §6).

**Evaluation metric.** Since the camera is mounted in a static position, we evaluate the attack effectiveness directly using the steering angle decision at the frame level instead of the end-to-end lateral deviation used in previous sections. This is equivalent from the attack effectiveness point of view since the large end-to-end lateral deviation is essentially created by a sequence of large steering angle decisions at the frame level. Specifically, we first find the camera frame that has the same relative position between the camera and the patch as that in the miniature-scale experimental setup. Then we compare its *designed* steering angle at the attack generation time and its *observed* steering angle that the ALC system in OpenPilot intends to apply to the vehicle in the miniature-scale experiment. Thus, the more similar these two steering angles are, the higher realizability our attack has in the physical world.

**Road patch generation.** We follow the methodology in §4.3.5 to obtain and apply the color mapping in our experimental setup. The patch size is set to represent a 4.8-meter wide and 12-meter long one in the real world scale. Since the EON is static in our settings, we use the driving trajectory generated by a production-level AV simulator for the same scenario (the highway scenario in Table 4, detailed later in §6) in our motion model based input generation. The other parameters are set the same as those in §5.2.

**Attack results.** Fig. 11 shows a visualization of the lane detection results of the benign and attacked scenarios in the miniature-scale experiment using the OpenPilot’s official visualization tool. It visualizes the detected lane lines and the desired driving path that the ALC system will follow based on the lane detection results. As shown, in the benign scenario, both detected lane lines align accurately with the actual lane lines on the miniature-scale road, and the desired driving path is straight as expected. However, when the malicious road patch is placed, it bends the detected lane lines significantly to the left and causes the desired driving path to be curving to the left, which is exactly the designed attack effect of our lane-bending objective function (§4.3.2). In this case, the designed steering angle is 23.4 degrees to the left in the attack generation time, and the observed one in the miniature-scale experiment is 22.3 degrees to the left, which only differs by 4.7%. In contrast, in the benign scenario the observed steering angle for the same frame is 0.9 degrees to the right. This thus concretely demonstrates that our attack is robust to the 3 main practical factors when performed in the physical world, which thus has high realizability in practice.

## 6 END-TO-END ATTACK EVALUATION

To concretely understand the end-to-end security/safety implications of our attack, in this section we construct and evaluate on real-world attack scenarios using a production-grade simulator.

**Evaluation methodology.** For safety and ethical considerations, we perform evaluation in a production-grade Autonomous Driving (AD) simulator called LGSVL [54]. LGSVL is an open-source Unity-based simulator designed specifically for evaluating production-level AD systems. It leverages Unity’s built-in physics engine to accurately simulate the vehicle dynamics and tire-road interaction, and provide photo-realistic simulation of the driving environment. It has already been demonstrated [69] to be able to support production-grade AD systems such as Baidu Apollo [48] and Autoware [70]. The original LGSVL simulator does not support OpenPilot, and thus we implemented the bridging between them (i.e., passing actuation commands and sensor data to each other) on our own. In this process we overcame engineering challenges such as the sensing/actuation channel interfacing and control interruption mechanism modifications, which are detailed in Appendix E. This is an engineering contribution of this paper and we will open source it to benefit the community.

**End-to-end attack scenario design.** We construct 2 end-to-end attack scenarios for highway and local road settings respectively, which are shown in Fig. 12. As shown, for the highway one, we place a concrete barrier on the left to the victim’s lane, and

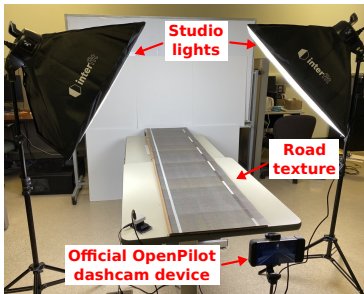


Figure 10: Miniature-scale experiment setup. Road texture/patch are printed on ledger-size papers.

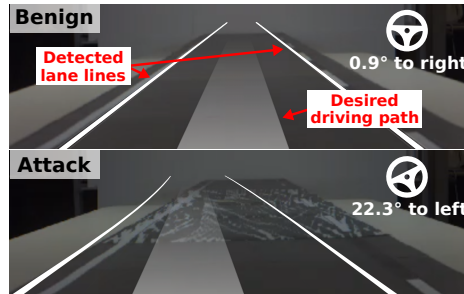


Figure 11: Lane detection and steering angle decisions in benign and attacked scenarios in the miniature-scale experiment.

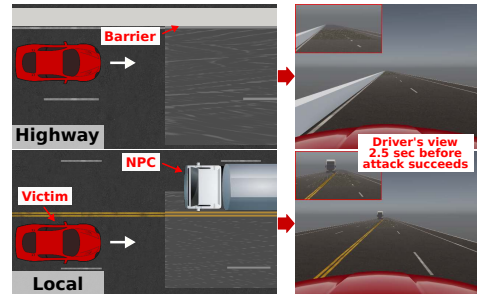


Figure 12: End-to-end attack scenarios and driver's view 2.5 sec before attack succeeds in simulation. Larger images are in Fig. 16.

**Table 4: Simulation scenario configurations and evaluation results. Lane widths and vehicle speeds are based on standard/common ones in the U.S. [71]. Simulation results without attack are confirmed to have 0% success rates with  $\leq 0.018$  m (std:  $\leq 9e-4$ ) average maximum deviations.**

Sim. Scenario	Lane Width	Veh. Speed	Attack Goal	Ave. Max Dev.	Succ. Rate	Succ. Time
Highway	3.6 m	65 mph (29 m/s)	Hit the concrete barrier on the left	0.67 m (std: $1e-2$ )	98% (98/100)	0.7 s
Local	2.7 m	45 mph (20 m/s)	Hit the truck in the opposite direction	0.90 m (std: $3e-2$ )	100% (100/100)	1.15 s

for the local road one, we place an NPC (Non-Player Character) truck driving on an opposite direction lane adjacent to the victim's. The attack goals for them are to hit the concrete barrier and the truck respectively, which thus both directly have severe safety consequences. For each scenario, we design the detailed scenario configurations such as lane markings, vehicle speed, and lane width according to the common settings of the given driving scenario in the real world. Detailed scenario configurations are listed in Table 4.

**Experimental setup and evaluation metrics.** We perform evaluation on the LGSVL-OpenPilot bridge we developed for OpenPilot v0.6.6. Due to the high engineering efforts in developing the bridge, we did not evaluate on v0.7.0. However, as shown in §5.3, the v0.6.6 LD model is actually more robust than the v0.7.0 one and thus our evaluation results should be applicable to v0.7.0. In the simulation, we use the Toyota RAV4 parameters in OpenPilot.

Since LGSVL provides photo-realistic simulation of the lighting condition, it also has a color distortion effect similar to the physical world. Thus, we follow the methodology in §4.3.5 to obtain and apply the color mapping in our simulation environment. The patch size is designed to be 5.4 m wide and 96 m long in the simulation scale. The other parameter settings are the same as §5.3. The road patches are placed at least 100 m away from the victim's starting position so that the simulation starts from a benign state where the patch is completely unnoticeable in the camera. For each scenario, we repeat the simulation for 100 times, and a successful attack is defined as achieving the corresponding attack goals in Table 12. we use the simulation logs to determine whether the victim vehicle body has an intersection with the barrier or the truck body.

**Results and attack demos.** As shown in Table 4, our attack achieves 98% and 100% for the highway and local road scenarios respectively, which shows a high end-to-end attack effectiveness. For the highway scenario, our attack fails 2 of the 100 runs. In these 2,

the deviations are still quite large and both are  $\leq 0.1$  m away from hitting the concrete barrier. Such slight vehicle trajectory differences across multiple runs are likely caused by simulation randomness, e.g., from the physics engine and messaging delay/dropping.

We record demo videos for both attack scenarios from the simulation experiments, available at <https://sites.google.com/view/cav-sec/alc-adv-attack>. In the highway scenario, after the victim hits the concrete barrier, it bounces away quickly due to the abrupt collision. In the local road one, the victim crashes to the front of the truck, causing a full stop for both the victim and truck. Such simulation results look highly dangerous and can be fatal, which thus concretely demonstrate the severe end-to-end safety consequences of our attack. Snapshots of the demo when the attack goals are achieved are in Fig. 14 in the Appendix.

In the simulation, the attack happens very fast: in  $\sim 1$  sec, the victim is already deviated out of the lane boundary. Similar to our conclusion in §5.1, this means that even if the driver notices the attack when the vehicle starts to deviate, it is already too late given the 2.5-sec average driver reaction time (Appendix A). Moreover, such crash cannot be prevented from the truck driver side since the truck driver also does not have enough reaction time to yield.

**Stealthiness.** To understand the attack stealthiness, we show the camera frames from the driver's view 2.5 sec before the attack succeeds on the right of Fig. 12. Similar to the results in §5.1, in the highway scenario the patch is almost invisible and in the local road scenario it looks to have similar or smaller white dirty patterns compared to the normal real-world ones such as those in Fig. 9. However, if the human driver is not alerted and takes over at this point, she misses the last chance to prevent the crash.

## 7 LIMITATIONS AND DEFENSE DISCUSSION

### 7.1 Limitations of Our Study

**Attack deployability.** Our current design mainly focuses on attack effectiveness and robustness in the physical world but does not systematically optimize its deployability. For example, in §5 and §6, the malicious road patch sizes we currently use are at least 3.6-meter wide and 24-meter long. This does not render our attack undeployable though, since the attacker can (1) use adhesive road patches (Fig. 2) to make the deployment quicker, (2) pretend to be road works to make the deployment to appear more legitimate, (3) pick a deployment time when the target road is the most vacant, e.g., in late night, and (4) break the entire patch into smaller pieces

and deploy them one at a time to avoid drawing too much attention. Nevertheless, smaller patch sizes can still generally make the deployment process easier and thus increase the practicality of our attack. One idea we plan to explore is to constrain the perturbations to only a few most effective small regions inside the current patch area in the optimization, so that the attacker only need to deploy patches to these small regions, instead of the entire patch area.

**Practicality evaluation.** In this work, we did not perform evaluation with real vehicles on real roads due to legal, safety, and ethical concerns as discussed in §5.4. This thus makes it still unclear how effective our attack can actually perform in the real world. Nevertheless, we tried our best to reach the limit of any academic research works by evaluating our attack against various possible real-world factors such as motion model inaccuracies, lighting conditions, printer color accuracy, and camera sensing capability (§5.2 and §5.4). To more concretely understand its end-to-end safety implications without incurring safety concerns, we also evaluate our attack on concrete real-world attack scenarios using a production-grade simulator (§6). Note that similar to us, companies such as Waymos and Uber also heavily rely on trace-based and simulation-based evaluations when developing and testing their driving automation systems for safety and budget considerations [72–74].

**Generality evaluation.** Although we have shown high attack generality against LD models with different designs (§5.3), all our evaluations are performed on only one production ALC system in OpenPilot. Thus, it is still unclear whether other popular ALC systems, e.g., Tesla Autopilot and GM Cruise, are vulnerable to our attack. Unfortunately, to the best of our knowledge, the OpenPilot ALC system is the only production one that is open sourced, and it is unlikely for these other companies to do so in the near future. Nevertheless, since the OpenPilot ALC system is representative at both design and implementation levels (§5), we believe that as the first study our current discovery and evaluation results can already most generally benefit the understanding of the security of state-of-the-art ALC systems today. Also, since DNN models are generally vulnerable to adversarial attacks [4–7, 11, 31–36, 52], if these other ALC systems also adopt the state-of-the-art DNN-based design, at least at design level they are also vulnerable to our attack.

## 7.2 Defense Discussion

**Machine learning model level defenses.** In the recent arms race between adversarial machine learning attacks and defenses, numerous defense/mitigation techniques have been proposed, e.g., model ensembling [75], randomization [76, 77], image transformation [78–81], and adversarial training [53]. However, so far none of them can guarantee general high effectiveness in practice, and the newly-proposed ones are constantly being defeated over time [66, 82]. Moreover, these prior works concentrate on image classification and object detection models, which thus cannot directly be applied to LD models. Thus, in the defense direction, we plan to first explore domain-specific adaptations of existing defense strategies in other application domains to LD models, and then leverage the insights to design effective solutions specific to our problem setting.

**Sensor/data fusion based defenses.** Besides securing the LD models, another defense direction is to fuse camera-based lane detection with other independent sensor/data sources such as LiDAR

and High Definition (HD) map [83]. For example, although LiDAR is generally designed for measuring distances instead of recognizing colors, it can actually capture the tiny light reflection differences between road surface with and without lane line markings, and thus is possible to perform lane detection [84]. However, due to its high cost, to the best of our knowledge, none of the production ALC systems today are equipped with LiDAR [3, 12, 27]. Moreover, Elon Musk, the co-founder of Tesla, claims that LiDARs are “*expensive sensors that are unnecessary (for autonomous vehicles)*” [85].

Another possible fusion source is lane information from an HD map, which is a technology used in production-level high-autonomy (e.g., Level-4) autonomous driving systems [48, 86]. However, to obtain accurate lane information from an HD map, an accurate positioning of the vehicle in such a map is needed in the first place, and the state-of-the-art solution of such positioning is still based on LiDAR [87–93]. While LiDAR is indeed not very cost-effective for normal operations, our results show that camera-based lane detection alone is actually not secure enough. Thus, we hope that the findings and insights in this paper can bring attention and motivate the consideration of incorporating LiDAR or other sensors useful for lane detection into future ALC systems.

## 8 RELATED WORK

**Autonomous Driving (AD) system security.** Recently, researchers have started to study the security of AD systems due to their increasing popularity. Since AD systems heavily rely on sensors, prior works have studied *sensor attacks* in AD context such as spoofing/jamming attacks on camera [94–96], LiDAR [94, 97, 98], radar [95], ultrasonic [95], and IMU [99, 100]. In comparison, these works mainly focus on vulnerabilities at the sensor level, while we focus on those at the higher *autonomy software* level, i.e., the “brain” of AD systems. At the autonomy software level, prior works have studied the security of camera/LiDAR-based object detection [5–7, 98, 101] and tracking [102], and end-to-end AD models [37–40]. Regarding our focus, production-level ALC systems, the only prior effort is from Tencent [9]. However, unlike us, as discussed in §1 it neither attacks the designed operational domain for ALC systems (i.e., roads with lane lines), nor generates perturbations systematically by addressing any of the 3 design challenges in §3.3.

**Digital-space adversarial attacks.** Since Szegedy *et al.* [11] first discovered the existence of adversarial examples, a huge number of adversarial attack methods have been proposed to generate adversarial examples in the digital image space [31, 52, 53, 103, 104]. In comparison, we focus on adversarial attacks realizable in the physical world against production DNN-based systems, which requires to address various new design challenges (§3.3, §4).

**Physical-world adversarial attacks.** Multiple prior works have explored image-space adversarial attacks in the physical world [5–7, 32–36, 105]. In particular, various techniques have been designed to improve the physical-world robustness, e.g., non-printability score [5, 6, 33, 36] and low-saturation colors [7] for printer color distortion, and EoT for camera angle and distance changes [5–7, 34, 35]. In comparison, prior efforts concentrate on image classification and object detection, while we are the first to systematically design physical-world adversarial attacks on ALC systems, which requires to address various new and unique design challenges (§3.3).



## 9 CONCLUSION

In this work, we are the first to systematically study the security of DNN-based ALC systems in their designed operational domains under physical-world adversarial attacks. We identify a novel attack vector, dirty road patches, and perform optimization-based attack generation with novel designs such as motion model based input generation and lane-bending objective function. Attack evaluation on a production ALC system using real-world driving traces shows that our attack has over 92% success rates with success time substantially lower than the average driver reaction time, and is also robust to motion model inaccuracies, different LD model designs, and physical-world factors. We further evaluate on concrete real-world attack scenarios using simulation, and find that our attack can cause severe end-to-end safety consequences. We also discuss defense directions. Considering the popularity of ALC systems and the severe security/safety implications shown in this paper, we hope that our findings and insights can bring community attention and inspire the development of effective defenses in practice.

## REFERENCES

- [1] SAE international. Taxonomy and Definitions for Terms Related to Driving Automation Systems for On-Road Motor Vehicles. *SAE International*,(J3016), 2016.
- [2] The tuSimple Lane Challenge. <http://benchmark.tusimple.ai/>, 2017.
- [3] Tesla Autopilot. <https://www.tesla.com/autopilot>, 2020.
- [4] Kevin Eykholt, Ivan Evtimov, Earlece Fernandes, Bo Li, Amir Rahmati, Chaowei Xiao, Atul Prakash, Tadayoshi Kohno, and Dawn Song. Robust Physical-World Attacks on Deep Learning Visual Classification. In *Proceedings of the IEEE Conference on Computer Vision and Pattern Recognition (CVPR)*, 2018.
- [5] Kevin Eykholt, Ivan Evtimov, Earlece Fernandes, Bo Li, Amir Rahmati, Florian Tramer, Atul Prakash, Tadayoshi Kohno, and Dawn Song. Physical Adversarial Examples for Object Detectors. In *12th USENIX Workshop on Offensive Technologies (WOOT 18)*, 2018.
- [6] Shang-Tse Chen, Cory Cornelius, Jason Martin, and Duen Horng Polo Chau. Shapeshifter: Robust Physical Adversarial Attack on Faster R-CNN Object Detector. In *Joint European Conference on Machine Learning and Knowledge Discovery in Databases*, pages 52–68. Springer, 2018.
- [7] Yue Zhao, Hong Zhu, Ruigang Liang, Qintao Shen, Shengzhi Zhang, and Kai Chen. Seeing isn't Believing: Practical Adversarial Attack Against Object Detectors. In *ACM SIGSAC Conference on Computer and Communications Security (ACM CCS)*, page 1989a–1990a, 2019.
- [8] California Penal Code 594 PC. [https://leginfo.ca.gov/faces/codes\\_displaySection.xhtml?lawCode=PEN&sectionNum=594](https://leginfo.ca.gov/faces/codes_displaySection.xhtml?lawCode=PEN&sectionNum=594), 1872.
- [9] Experimental Security Research of Tesla Autopilot. [https://keenlab.tencent.com/en/whitepapers/Experimental\\_Security\\_Research\\_of\\_Tesla\\_Autopilot.pdf](https://keenlab.tencent.com/en/whitepapers/Experimental_Security_Research_of_Tesla_Autopilot.pdf), 2019.
- [10] Tesla Autopilot Support. <https://www.tesla.com/support/autopilot>, 2020.
- [11] Christian Szegedy, Wojciech Zaremba, Ilya Sutskever, Joan Bruna, Dumitru Erhan, Ian Goodfellow, and Rob Fergus. Intriguing Properties of Neural Networks. In *International Conference on Learning Representation (ICLR)*, 2014.
- [12] OpenPilot: Open Source Driving Agent. <https://github.com/commaai/openpilot>, 2018.
- [13] Is a \$1000 Aftermarket Add-On as Capable as Tesla's Autopilot and Cadillac's Super Cruise? <https://www.caranddriver.com/features/a30341053/self-driving-technology-comparison/>, 2020.
- [14] We hit the road with Comma.ai's assisted-driving tech at CES 2020. <https://www.cnet.com/roadshow/news/comma-ai-assisted-driving-george-hotz-ces-2020/>, 2020.
- [15] Hands-on with Comma.ai's add-on Level 2 autonomous tech. <https://www.cnet.com/roadshow/news/hands-on-with-comma-ais-add-on-level-2-autonomous-tech/>, 2018.
- [16] Lane Keeping Assist System Using Model Predictive Control. <https://www.mathworks.com/help/mpc/ug/lane-keeping-assist-system-using-model-predictive-control.html>, 2020.
- [17] Jin-Woo Lee and Bakhtiar Litkouhi. A Unified Framework of the Automated Lane Centering/Changing Control for Motion Smoothness Adaptation. In *2012 15th International IEEE Conference on Intelligent Transportation Systems*, pages 282–287. IEEE, 2012.
- [18] Aharon Bar Hillel, Ronen Lerner, Dan Levi, and Guy Raz. Recent Progress in Road and Lane Detection: A Survey. *Machine vision and applications*, 25(3):727–745, 2014.
- [19] Ze Wang, Weiqiang Ren, and Qiang Qiu. LaneNet: Real-Time Lane Detection Networks for Autonomous Driving. *arXiv preprint arXiv:1807.01726*, 2018.
- [20] Xingang Pan, Jianping Shi, Ping Luo, Xiaogang Wang, and Xiaoou Tang. Spatial as Deep: Spatial CNN for Traffic Scene Understanding. In *Thirty-Second AAAI Conference on Artificial Intelligence*, 2018.
- [21] Yeongmin Ko, Jiwon Jun, Donghwuy Ko, and Moongu Jeon. Key Points Estimation and Point Instance Segmentation Approach for Lane Detection, 2020.
- [22] Jun Li, Xue Mei, Danil Prokhorov, and Dacheng Tao. Deep Neural Network for Structural Prediction and Lane Detection in Traffic Scene. *IEEE transactions on neural networks and learning systems*, 28(3):690–703, 2016.
- [23] Qin Zou, Hanwen Jiang, Qiyu Dai, Yuanhao Yue, Long Chen, and Qian Wang. Robust Lane Detection From Continuous Driving Scenes Using Deep Neural Networks. *IEEE Transactions on Vehicular Technology*, PP:1–1, 10 2019.
- [24] Peer Smuda, Roland Schweiger, Heiko Neumann, and Werner Ritter. Multiple Cue Data Fusion With Particle Filters for Road Course Detection in Vision Systems. In *2006 IEEE Intelligent Vehicles Symposium*, pages 400–405. IEEE, 2006.
- [25] Christina Gackstatter, Patrick Heinemann, Sven Thomas, and Gudrun Klinker. Stable Road Lane Model Based on Clothoids. In *Advanced Microsystems for Automotive Applications 2010*, pages 133–143. Springer, 2010.
- [26] Sibel Yenikaya, Gökhan Yenikaya, and Ekrem Düven. Keeping the Vehicle on the Road - A Survey on On-Road Lane Detection Systems. *ACM Computing Surveys (CSUR)*, 46(1):1–43, 2013.
- [27] Christopher Becker, Larry J. Yount, Shane Rozen-Levy, and John David Brewer. Functional Safety Assessment of an Automated Lane Centering System. In *National Highway Traffic Safety Administration*, 2018.

- [28] Richard C Dorf and Robert H Bishop. *Modern Control Systems*. Pearson, 2011.
- [29] Richalet, J. and Rault, A. and Testud, J. L. and Papon, J. Paper: Model Predictive Heuristic Control. *Automatica*, 14(5):413–428, September 1978.
- [30] Tinkla: Tinkering with Tesla. <https://tinkla.us/>, 2018.
- [31] Ian J Goodfellow, Jonathon Shlens, and Christian Szegedy. Explaining and Harnessing Adversarial Examples. *arXiv preprint arXiv:1412.6572*, 2014.
- [32] Alexey Kurakin, Ian Goodfellow, and Samy Bengio. Adversarial Examples in the Physical World. *arXiv preprint arXiv:1607.02533*, 2016.
- [33] Mahmood Sharif, Sruti Bhagavatula, Lujo Bauer, and Michael K Reiter. Accessorize to a Crime: Real and Stealthy Attacks on State-of-the-Art Face Recognition. In *Proceedings of the 2016 ACM SIGSAC conference on computer and communications security*, CCS '16, pages 1528–1540, 2016.
- [34] Anish Athalye, Logan Engstrom, Andrew Ilyas, and Kevin Kwok. Synthesizing Robust Adversarial Examples. In *Proceedings of the 35th International Conference on Machine Learning (ICML)*, 2018.
- [35] Tom Brown, Dandelion Mane, Aurko Roy, Martin Abadi, and Justin Gilmer. Adversarial Patch. *arXiv preprint arXiv:1712.09665*, 2017.
- [36] Zhenyu Zhong, Weilin Xu, Yunhan Jia, and Tao Wei. Perception Deception: Physical Adversarial Attack Challenges and Tactics for DNN-Based Object Detection. In *Black Hat Europe*, 2018.
- [37] Kexin Pei, Yinzhi Cao, Junfeng Yang, and Suman Jana. Deepxplore: Automated Whitebox Testing of Deep Learning Systems. In *proceedings of the 26th Symposium on Operating Systems Principles*, pages 1–18, 2017.
- [38] Yuchi Tian, Kexin Pei, Suman Jana, and Baishakhi Ray. Deeptest: Automated Testing of Deep-Neural-Network-Driven Autonomous Cars. In *International Conference on Software Engineering*, pages 303–314, 2018.
- [39] Alesia Chemikova, Alina Oprea, Cristina Nita-Rotaru, and BaekGyu Kim. Are Self-Driving Cars Secure? Evasion Attacks against Deep Neural Networks for Steering Angle Prediction. In *2019 IEEE Security and Privacy Workshops (SPW)*, pages 132–137. IEEE, 2019.
- [40] Husheng Zhou, Wei Li, Yuankun Zhu, Yuqun Zhang, Bei Yu, Lingming Zhang, and Cong Liu. Deepbillboard: Systematic Physical-World Testing of Autonomous Driving Systems. In *International Conference on Software Engineering*, 2020.
- [41] State of California Department of Motor Vehicles. *California Commercial Driver Handbook: Section 2 – Driving Safely*. 2019. Available at <https://www.dmv.ca.gov/portal/dmv/detail/pubs/cdl.htm#sec2>.
- [42] UK ACPO Road Policing Enforcement Technology Committee. *ACPO Code of Practice for Operational use of Enforcement Equipment*. 2002.
- [43] UK Department for Transport. *The Official Highway Code Book*. 2015.
- [44] National Safety Council. *Reference Material for DDC Instructors, 5th Edition*. 2005.
- [45] California Vehicle Code 21663. [https://leginfo.ca.gov/faces/codes\\_displaySection.xhtml?lawCode=VEH&sectionNum=21663](https://leginfo.ca.gov/faces/codes_displaySection.xhtml?lawCode=VEH&sectionNum=21663), 1959.
- [46] Does your car have automated emergency braking? It's a big fail for pedestrians. <https://www.zdnet.com/article/does-your-car-have-automated-emergency-braking-its-a-big-fail-for-pedestrians/>, 2019.
- [47] Rajesh Rajamani. *Vehicle Dynamics and Control*. Springer Science & Business Media, 2011.
- [48] Baidu Apollo. <https://github.com/ApolloAuto/apollo>, 2017.
- [49] Nicholas Carlini and David Wagner. Audio Adversarial Examples: Targeted Attacks on Speech-to-Text. In *2018 IEEE Security and Privacy Workshops (SPW)*, pages 1–7. IEEE, 2018.
- [50] Javid Ebrahimi, Daniel Lowd, and Dejing Dou. On Adversarial Examples for Character-Level Neural Machine Translation. In *Proceedings of the 27th International Conference on Computational Linguistics (COLING)*. Association for Computational Linguistics, 2018.
- [51] Adhesive Patch can Seal Potholes and Cracks on the Road. <https://www.startupsellie.net/2019/05/07/american-road-patch-seals-potholes-road-cracks/>, 2019.
- [52] Nicholas Carlini and David Wagner. Towards Evaluating the Robustness of Neural Networks. In *2017 IEEE Symposium on Security and Privacy (SP)*, pages 39–57. IEEE, 2017.
- [53] Aleksander Madry, Aleksandar Makelov, Ludwig Schmidt, Dimitris Tsipras, and Adrian Vladu. Towards Deep Learning Models Resistant to Adversarial Attacks. In *International Conference on Learning Representation (ICLR)*, 2018.
- [54] LGSVL Simulator: An Autonomous Vehicle Simulator. <https://github.com/lgsvl/simulator/>, 2018.
- [55] Alexey Dosovitskiy, German Ros, Felipe Codevilla, Antonio Lopez, and Vladlen Koltun. CARLA: An Open Urban Driving Simulator. In *Annual Conference on Robot Learning*, 2017.
- [56] Richard Hartley and Andrew Zisserman. *Multiple View Geometry in Computer Vision*. Cambridge University Press, 2 edition, 2003.
- [57] Shiho Tanaka, Kenichi Yamada, Toshio Ito, and Takenao Ohkawa. Vehicle Detection Based on Perspective Transformation Using Rear-View Camera. *Hindawi Publishing Corporation International Journal of Vehicular Technology*, 9, 03 2011.
- [58] Dragomir Anguelov, Carole Dulong, Daniel Filip, Christian Frueh, Stéphane Lafon, Richard Lyon, Abhijit Ogale, Luc Vincent, and Josh Weaver. Google Street View: Capturing the World at Street Level. *Computer*, 43(6):32–38, 2010.
- [59] Jason Kong, Mark Pfeiffer, Georg Schildbach, and Francesco Borrelli. Kinematic and Dynamic Vehicle Models for Autonomous Driving Control Design. In *2015 IEEE Intelligent Vehicles Symposium (IV)*, pages 1094–1099. IEEE, 2015.
- [60] Introduction to Self-Driving Cars. <https://www.coursera.org/learn/intro-self-driving-cars>, 2019.
- [61] Daniel Watznig and Martin Horn. *Automated driving: safer and more efficient future driving*. Springer, 2016.
- [62] Diederik P Kingma and Jimmy Ba. Adam: A Method for Stochastic Optimization. In *International Conference on Learning Representation (ICLR)*, 2015.
- [63] Eric Hamilton. JPEG file interchange format. 2004.
- [64] Harald Schafer, Eder Santana, Andrew Haden, and Riccardo Biasini. A Commute in Data: The comma2k19 Dataset. *arXiv preprint arXiv:1812.05752*, 2018.
- [65] Xiang Ling, Shouling Ji, Jiaxu Zou, Jiannan Wang, Chunming Wu, Bo Li, and Ting Wang. Deepsec: A Uniform Platform for Security Analysis of Deep Learning Model. In *2019 IEEE Symposium on Security and Privacy (SP)*, pages 673–690. IEEE, 2019.
- [66] Anish Athalye, Nicholas Carlini, and David Wagner. Obfuscated Gradients Give a False Sense of Security: Circumventing Defenses to Adversarial Examples. In *Proceedings of the 35th International Conference on Machine Learning (ICML)*, 2018.
- [67] Angus Galloway, Anna Golubeva, Thomas Tanay, Medhat Moussa, and Graham W Taylor. Batch Normalization is a Cause of Adversarial Vulnerability. *arXiv preprint arXiv:1905.02161*, 2019.
- [68] TOYOTA SAFETY SENSE P: Features and Operation Overview. [https://www.toyota.com/content/ebrochure/CFA\\_TSS\\_P.pdf](https://www.toyota.com/content/ebrochure/CFA_TSS_P.pdf), 2018.
- [69] LGSVL Simulator Overview. <https://www.lgsvlsimulator.com/downloads/LGSVL-Simulator-Overview.pdf>, 2019.
- [70] Shinpei Kato, Shota Tokunaga, Yuya Maruyama, Seiya Maeda, Manato Hirabayashi, Yuki Kitsukawa, Abraham Monroy, Tomohito Ando, Yusuke Fujii, and Takuya Azumi. Autoware On Board: Enabling Autonomous Vehicles with Embedded Systems. In *ICCPs'18*, pages 287–296. IEEE Press, 2018.
- [71] American Association of State Highway and Transportation Officials (AASHTO). *Policy on Geometric Design of Highways and Streets (7th Edition)*. American Association of State Highway and Transportation Officials (AASHTO), 2018.
- [72] Simulation Becomes Increasingly Important For Self-Driving Cars. <https://www.forbes.com/sites/davidsilver/2018/11/01/simulation-becomes-increasingly-important-for-self-driving-cars/>, 2018.
- [73] Inside Waymo's Secret World for Training Self-Driving Cars. <https://www.theatlantic.com/technology/archive/2017/08/inside-waymos-secret-testing-and-simulation-facilities/537648/>, 2017.
- [74] Simulation Engine from MIT Trains Self-Driving Cars Before They Hit Real roads. <https://www.therobotreport.com/simulation-engine-mit-trains-self-driving-cars-before-hit-real-streets/>, 2020.
- [75] Florian Tramèr, Alexey Kurakin, Nicolas Papernot, Ian Goodfellow, Dan Boneh, and Patrick McDaniel. Ensemble Adversarial Training: Attacks and Defenses. In *International Conference on Learning Representation (ICLR)*, 2018.
- [76] Yuchen Zhang and Percy Liang. Defending Against Whitebox Adversarial Attacks via Randomized Discretization. In *International Conference on Artificial Intelligence and Statistics (AISTATS)*, 2019.
- [77] Cihang Xie, Jianyu Wang, Zhishuai Zhang, Zhou Ren, and Alan Yuille. Mitigating Adversarial Effects Through Randomization. *arXiv preprint arXiv:1711.01991*, 2017.
- [78] Fangzhou Liao, Ming Liang, Yinpeng Dong, Tianyu Pang, Xiaolin Hu, and Jun Zhu. Defense Against Adversarial Attacks Using High-Level Representation Guided Denoiser. In *Proceedings of the IEEE Conference on Computer Vision and Pattern Recognition (CVPR)*, pages 1778–1787, 2018.
- [79] Cihang Xie, Yuxin Wu, Laurens van der Maaten, Alan L Yuille, and Kaiming He. Feature Denoising for Improving Adversarial Robustness. In *Proceedings of the IEEE Conference on Computer Vision and Pattern Recognition (CVPR)*, pages 501–509, 2019.
- [80] Weilin Xu, David Evans, and Yanjun Qi. Feature Squeezing: Detecting Adversarial Examples in Deep Neural Networks. *arXiv preprint arXiv:1704.01155*, 2017.
- [81] Chuan Guo, Mayank Rana, Moustapha Cisse, and Laurens Van Der Maaten. Countering Adversarial Images using Input Transformations. In *International Conference on Learning Representation (ICLR)*, 2018.
- [82] Florian Tramèr, Nicholas Carlini, Wieland Brendel, and Aleksander Madry. On Adaptive Attacks to Adversarial Example Defenses. *arXiv preprint arXiv:2002.08347*, 2020.
- [83] HD Maps: New Age Maps Powering Autonomous Vehicles. <https://www.geospatialworld.net/article/hd-maps-autonomous-vehicles/>.
- [84] Min Bai, Gellert Mattyus, Namdar Homayounfar, Shenlong Wang, Shrinidhi Kowshika Lakshmikanth, and Raquel Urtasun. Deep multi-sensor lane detection. In *2018 IEEE/RSJ International Conference on Intelligent Robots and Systems (IROS)*, pages 3102–3109. IEEE, 2018.
- [85] 'Anyone relying on lidar is doomed,' Elon Musk says. <https://techcrunch.com/2019/04/22/anyone-relying-on-lidar-is-doomed-elon-musk-says/>, 2019.

- [86] Building Maps for a Self-Driving Car. <https://link.medium.com/Bo5pCOov95>, 2016.
- [87] Self-Driving Car Engineer Nanodegree. <https://www.udacity.com/course/self-driving-car-engineer-nanodegree--nd013>.
- [88] Self-Driving Fundamentals: Featuring Apollo. <https://www.udacity.com/course/self-driving-car-fundamentals-featuring-apollo--ud0419>.
- [89] Guowei Wan, Xiaolong Yang, Renlan Cai, Hao Li, Yao Zhou, Hao Wang, and Shiyu Song. Robust and Precise Vehicle Localization based on Multi-Sensor Fusion in Diverse City Scenes. In *ICRA*, pages 4670–4677. IEEE, 2018.
- [90] Yanbin Gao, Shifei Liu, Mohamed Atia, and Aboelmagd Noureldin. INS/GPS/LiDAR Integrated Navigation System for Urban and Indoor Environments Using Hybrid Scan Matching Algorithm. *Sensors*, 15(9):23286–23302, 2015.
- [91] Fabian de Ponte Müller. Survey on Ranging Sensors and Cooperative Techniques for Relative Positioning of Vehicles. *Sensors*, 17(2):271, 2017.
- [92] Jesse Levinson and Sebastian Thrun. Robust Vehicle Localization in Urban Environments Using Probabilistic Maps. In *2010 IEEE International Conference on Robotics and Automation*, pages 4372–4378. IEEE, 2010.
- [93] Andrey Soloviev. Tight Coupling of GPS, Laser Scanner, and Inertial Measurements for Navigation in Urban Environments. In *IEEE/ION Position, Location and Navigation Symposium*. IEEE, 2008.
- [94] Jonathan Petit, Bas Stottelaar, Michael Feiri, and Frank Kargl. Remote Attacks on Automated Vehicles Sensors: Experiments on Camera and Lidar. *Black Hat Europe*, 11:2015, 2015.
- [95] Chen Yan, Wenyuan Xu, and Jianhao Liu. Can You Trust Autonomous Vehicles: Contactless Attacks Against Sensors of Self-Driving Vehicle. *DEF CON*, 24(8):109, 2016.
- [96] Ben Nassi, Dudi Nassi, Raz Ben-Netanel, Yisroel Mirsky, Oleg Drokin, and Yuval Elovici. Phantom of the ADAS: Phantom Attacks on Driver-Assistance Systems, 2020.
- [97] Hocheol Shin, Dohyun Kim, Yujin Kwon, and Yongdae Kim. Illusion and Dazzle: Adversarial Optical Channel Exploits Against Lidars for Automotive Applications. In *International Conference on Cryptographic Hardware and Embedded Systems*, pages 445–467. Springer, 2017.
- [98] Yulong Cao, Chaowei Xiao, Benjamin Cyr, Yimeng Zhou, Won Park, Sara Rampazzi, Qi Alfred Chen, Kevin Fu, and Z Morley Mao. Adversarial Sensor Attack on Lidar-Based Perception in Autonomous Driving. In *Proceedings of the 2019 ACM SIGSAC Conference on Computer and Communications Security, CCS '19*, pages 2267–2281, 2019.
- [99] Yazhou Tu, Zhiqiang Lin, Insup Lee, and Xiali Hei. Injected and Delivered: Fabricating Implicit Control over Actuation Systems by Spoofing Inertial Sensors. In *USENIX Security*, pages 1545–1562, 2018.
- [100] Timothy Trippel, Ofir Weisse, Wenyuan Xu, Peter Honeyman, and Kevin Fu. WALNUT: Waging Doubt on the Integrity of MEMS Accelerometers with Acoustic Injection Attacks. In *EuroS&P*, pages 3–18. IEEE, 2017.
- [101] Model Hacking ADAS to Pave Safer Roads for Autonomous Vehicles. <https://www.mcafee.com/blogs/other-blogs/mcafee-labs/model-hacking-adas-to-pave-safer-roads-for-autonomous-vehicles/>, 2020.
- [102] Yunhan Jia, Yantao Lu, Junjie Shen, Qi Alfred Chen, Hao Chen, Zhenyu Zhong, and Tao Wei. Fooling Detection Alone is Not Enough: Adversarial Attack Against Multiple Object Tracking. In *International Conference on Learning Representations*, 2019.
- [103] Nicolas Papernot, Patrick McDaniel, Somesh Jha, Matt Fredrikson, Z Berkay Celik, and Ananthram Swami. The Limitations of Deep Learning in Adversarial Settings. In *2016 IEEE European symposium on security and privacy (EuroS&P)*, pages 372–387. IEEE, 2016.
- [104] Seyed-Mohsen Moosavi-Dezfooli, Alhussein Fawzi, and Pascal Frossard. DeepFool: A Simple and Accurate Method to Fool Deep Neural Networks. In *Proceedings of the IEEE conference on computer vision and pattern recognition*, pages 2574–2582, 2016.
- [105] Juncheng Li, Frank Schmidt, and Zico Kolter. Adversarial Camera Stickers: A Physical Camera-based Attack on Deep Learning Systems. In *International Conference on Machine Learning*, pages 3896–3904, 2019.
- [106] Helen Loeb, Aditya Belwadi, Jalaj Maheshwari, and Saniyah Shaikh. Age and Gender Differences in Emergency Takeover from Automated to Manual Driving on Simulator. *Traffic injury prevention*, pages 1–3, 2019.
- [107] Watch Tesla Drivers Apparently Asleep at the Wheel, Renewing Autopilot Safety Questions. <https://www.cnbc.com/2019/09/09/watch-tesla-drivers-apparently-asleep-at-the-wheel-renewing-safety-questions.html>, 2019.
- [108] Kaiming He, Xiangyu Zhang, Shaoqing Ren, and Jian Sun. Deep Residual Learning for Image Recognition. In *Proceedings of the IEEE conference on computer vision and pattern recognition (CVPR)*, pages 770–778, 2016.
- [109] Kyunghyun Cho, Bart Van Merriënboer, Caglar Gulcehre, Dzmitry Bahdanau, Fethi Bougares, Holger Schwenk, and Yoshua Bengio. Learning Phrase Representations Using RNN Encoder-Decoder for Statistical Machine Translation. *arXiv preprint arXiv:1406.1078*, 2014.
- [110] Sepp Hochreiter and Jürgen Schmidhuber. Long Short-Term Memory. *Neural computation*, 9(8):1735–1780, 1997.
- [111] Yoshua Bengio, Patrice Simard, and Paolo Frasconi. Learning Long-Term Dependencies with Gradient Descent is Difficult. *IEEE transactions on neural networks*, 5(2):157–166, 1994.
- [112] Sergey Ioffe and Christian Szegedy. Batch Normalization: Accelerating Deep Network Training by Reducing Internal Covariate Shift. In *Proceedings of the 32nd International Conference on Machine Learning (ICML)*, 2015.
- [113] Jimmy Lei Ba, Jamie Ryan Kiros, and Geoffrey E Hinton. Layer Normalization. *arXiv preprint arXiv:1607.06450*, 2016.
- [114] Morgan Quigley, Ken Conley, Brian Gerkey, Josh Faust, Tully Foote, Jeremy Leibs, Rob Wheeler, and Andrew Y Ng. ROS: An Open-Source Robot Operating System. In *ICRA workshop on open source software*, volume 3, page 5. Kobe, Japan, 2009.
- [115] Pieter Hintjens. *ZeroMQ: Messaging for Many Applications*. O’Reilly Media, Inc., 2013.

## APPENDIX

### A REQUIRED DEVIATIONS AND SUCCESS TIME

**Required deviations.** The required deviations for the highway and local roads are calculated based on Toyota RAV4 width (including mirrors) and standard lane widths in the U.S. [71] as shown in Fig. 13. We use Toyota RAV4 since it is the reference vehicle used by the OpenPilot team when collecting the comma2k19 data set [64]. For the lane widths, we refer to the design guidelines [71] published by the U.S. Department of Transportation Federal Highway Administration. The required deviations to touch the lane line are calculated using  $\frac{L-C}{2} = 0.735m$  (highway) and  $0.285m$  (local), where  $L$  is the lane width and  $C$  is the vehicle width.

**Required success time.** Since ALC systems assume a fully attentive human driver who is prepared to take over at any moment [1, 10], the required deviation above needs to be achieved fast enough so that the human driver cannot react in time to take over and steer back. Thus, when we define the attack goal, we require not only the required deviation above, but also an attack success time that is smaller than the average driver reaction time to road hazards. We select the average driver reaction time based on different government-issued transportation policy guidelines [41–44]. In particular, in the California Department of Motor Vehicles Commercial Driver Handbook Section 2.6.1 [41], it describes (1) a 1.75 seconds *average perception time*, i.e., the time from the time the driver’s eyes see a hazard until the driver’s brain recognizes it, and (2) a 0.75 to 1 seconds *average reaction time*, i.e., the time from the driver’s brain recognizing the hazard to physically take actions. Thus, in total it’s **2.5 to 2.75 seconds** from the driver’s eyes seeing a hazard to physically take actions. The UK “Highway Code Book” and “Code of Practice for Operational Use of Road Policing Enforcement Technology” use 3 seconds for driver reaction time [42, 43]. National Safety Council also adopts a 3-second driver reaction time to calculate the minimum spacing between vehicles [44]. Among them, we select the **smallest** one, i.e., 2.5 seconds from the California Department of Motor Vehicles [41], as the required success time in this paper to avoid possible overestimation of the attack effectiveness in our evaluation.

Note that the driver reaction time above is commonly referring to the reaction time to apply the brake, instead of steering. In our paper, we use such reaction time to apply the brake as the reaction time to take over the steering wheel when the ALC systems is in control of the steering wheel. This is because in traditional driving, the driver is *actively* steering the vehicle but *passively* applying the

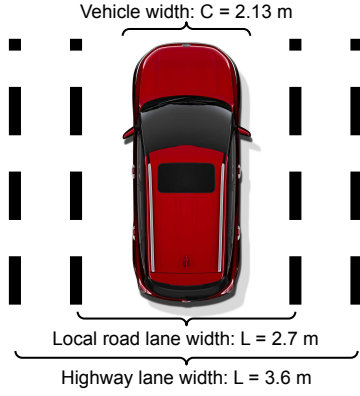


Figure 13: Vehicle and lane widths used in this paper.

brake. However, when the ALC system is controlling the steering, the human driver is *passively* steering the vehicle, i.e., her hands are not actively controlling the steering wheel. Thus, the reaction time to take over the steering wheel during passive steering is analogous to that to apply the brake during passive braking.

In fact, the actual average driver reaction time when the ALC system is taking control are likely to be much higher than the 2.5 seconds measured in tradition driving, due to the reliance of human drivers on such convenient driving automation technology today. A recent study performed a simulation-based user study on Tesla Autopilot, and found that 40% drivers fail to react in time to avoid a crash happening *6.2 seconds* after the Autopilot fails to operate [106]. In the real world, it is found multiple times that Tesla drivers fall asleep with Autopilot controlling the vehicle in high speed [107]. Thus, the required success time of 2.5 seconds used in this paper is a relatively conservative estimation, and thus the attack effectiveness reported in our evaluations is likely only a **lower bound** of the actual effectiveness of our attack in the real world.

## B DIFFERENTIABLE CONSTRUCTION OF THE CURVE FITTING PROCESS

Since the direct LD model output is the detected left and right lane line points (§2.1), a curve fitting step is further required to calculate  $\rho_t(d; \{X_j^a | j \leq t\})$  in Eq. 8 from the lane line points. This step also needs to be differentiable to allow the entire  $f(\cdot)$  differentiable by  $\{X_j^a | j \leq t\}$ . Thus, we further perform a differentiable construction of the curve fitting process as follows. We use  $P_l, P_r \in \mathbb{R}^{|D_t|}$  to represent the left and right lane line points respectively, where their indexes represent  $x$ -axis (longitudinal coordinate) and their values represent the  $y$ -axis (lateral coordinate). We first fit the lane line points into polynomial curves in a least-square manner with  $\xi_l = (V^T V)^{-1} V^T P_l$  and  $\xi_r = (V^T V)^{-1} V^T P_r$ , where  $\xi_l, \xi_r \in \mathbb{R}^{n+1}$  are the coefficients of the  $n$ -degree polynomial functions of the left and right lane lines respectively, and  $V \in \mathbb{R}^{|D_t| \times n+1}$  is a Vandermonde matrix. Then we calculate the desired driving path coefficients  $\xi_d$  by averaging those for the left and right lane lines:  $\xi_d = \frac{1}{2}(\xi_l + \xi_r)$ . As all operations above are written in closed form, the desired driving path polynomial  $\rho_t(d) = [1, d, d^2, \dots, d^n] \xi_d$  is differentiable by each lane line point.

Table 5: Evaluation results for attack robustness under different motion model inaccuracy levels.  $\Delta$  controls the errors introduced to lateral and longitudinal moving directions independently following the uniform distribution  $\mathcal{U}(-\Delta, \Delta)$ .

Error Level $\Delta$ (meter)	Highway		Local	
	Succ. rate	Succ. time (s)	Succ. rate	Succ. time (s)
0.012	97.5%	0.876	100%	0.926
0.024	97.5%	0.881	100%	0.767
0.048	97.5%	0.869	100%	0.814
0.096	95.0%	0.814	82.5%	0.797

## C ROBUSTNESS TO MOTION MODEL INACCURACIES

**Experimental setup.** According to previous studies, the errors of the kinematic bicycle model used in our attack are around 0.08 meters on average with a standard deviation of around 0.02 meters when the control frequency is 10 Hz (i.e., control applied every 100 ms) [59]. Since the control frequency in OpenPilot is 100 Hz, we estimate the errors in one control step (applied every 10 ms) as having 0.008 meters mean with 0.002 meters standard deviation. Based on this, in this section we evaluate the attack effectiveness with motion model errors randomly sampled from the uniform distribution  $U(-\Delta, \Delta)$  with  $\Delta = 0.012, 0.024, 0.048$  and  $0.096$ , which correspond to  $2\times, 4\times, 8\times,$  and  $16\times$  standard deviations respectively. These errors are added to the longitudinal and lateral position changes independently at each control step when we use the motion model to obtain the driving trajectory of the victim at the attack evaluation time. The evaluation dataset and metrics are the same as those in §5.1. The experiments use the same malicious road patches generated in §5.1 with  $\lambda = 10^{-3}$  and PAR=50%, the default stealthiness level as discussed in §5.1.

**Results.** Table 5 shows the attack success rates and time under each error level. As shown, even when the error level is 0.048 meters, our attack can still achieve 100% and 97.5% success rates for local road and highway scenarios respectively, and the average success time is still all under 0.95 sec. Such error level corresponds to 8 times the error standard deviation, or 8-sigma, meaning that an error higher than this only occurs once every  $10^{15}$  times. Since our attack on average takes less than 1 sec, or 100 control steps, such high attack effectiveness ( $\geq 97.5\%$  success rates) is almost always (a probability of  $1 - 10^{-13}$ ) robust to motion model errors that can occur during the attack. The success rate only drops significantly, but still over 80%, for local road scenarios when the error level is as high as 0.096 meters. Note that such error level means that in the worst case the motion model can have nearly 10 meters error per second, which is almost one half of a typical local road speed (e.g., 45 mph) and 35 times the required deviation for local road scenarios. Thus, this error level has significant effect on the attack effectiveness for local road scenarios. The attack effectiveness for highway scenarios is also affected, but much less than that for local road ones since the speed and required deviation for highway scenarios are higher.

## D DNN DESIGN DIFFERENCES FOR LD MODELS IN ATTACK GENERALITY EVALUATION (§5.3)

In §5.3, we select LD models from OpenPilot v0.7.0 (used in previous sections), v0.6.6, and v0.5.9 to perform generality evaluation considering their large DNN architecture differences with each other. Among them, the v0.5.9 model has the largest DNN architecture differences to the other two. First, the v0.5.9 model has 1.6 million trainable parameters and 49 layers, which are substantially smaller than the other models: 58% fewer weights and 58% fewer layers than the v0.7.0 model, and as high as 63% fewer weights and 60% fewer layers than the v0.6.6 model. At the design level, after a sequence of the CNN residual blocks [108], the v0.5.9 model uses a naive RNN layer [109], while the other two models use a more advanced RNN design called Gated Recurrent Unit (GRU). GRU is proposed to deal with long text in the natural language processing domain similar to LSTM [110] because the naive RNN is known to focus too much on the current and recent few words [111]. Thus, the v0.6.6 and v0.7.0 models with such more advanced RNN design should be able to consider more historical states and thus produce more stable results during driving.

Between v0.6.6 model and the v0.7.0 model, the former has 4.2 million weights and 124 layers, which are 11% more weights and 7% more layers than the latter and thus the largest among the three. A key design-level difference between them is that the Batch Normalization (BN) layer [112] is used in the v0.6.6 model but later removed in the v0.7.0 model, potentially because BN layers can harm RNN perform [113].

## E LGSVL-OPENPILOT BRIDGING

Since the original LGSVL simulator does not support OpenPilot, for the end-to-end safety consequence evaluation in §6 we have to implement the bridging between them (i.e., passing actuation decisions and sensor data to each other) on our own. Since OpenPilot is designed and optimized for a dedicated device (EON), in this process we overcome some engineering challenges detailed below. This is an engineering contribution of this paper, we will open source our LGSVL-OpenPilot bridge code to benefit future works in related research areas.

**Sensing/actuation channel interfacing.** Currently, LGSVL supports a ROS [114] based bridging to AD systems for receiving vehicle actuation commands and publishing simulated sensor data. However, since OpenPilot is built with a ZeroMQ [115] based messaging framework and has no existing support for simulation, we develop the interface to achieve a *frame-by-frame* simulation of OpenPilot driving in LGSVL. Such interface has 2 directions:

- (1) *Passing sensor data from LGSVL to OpenPilot.* OpenPilot is originally designed as a driving agent directly running on EON (the official OpenPilot dashcam). To support simulation, we modify OpenPilot such that it accepts camera frames from LGSVL instead of the native camera device driver on EON. After our modification, as soon as OpenPilot receives a camera frame, the lane detection, lateral control, and vehicle actuation logic in OpenPilot are triggered one by one as described in §2.1.



(a) Highway: hit concrete barrier. (b) Local: crash into a truck.

**Figure 14: Snapshots of the attack demo videos when the attack goals are achieved in the simulation for (a) the highway scenario, and (b) the local road scenario in the end-to-end safety consequence evaluation in §6.**

- (2) *Passing actuation commands from OpenPilot to LGSVL.* LGSVL allows the driving agent to control the built-in vehicle both laterally (i.e., steering) and longitudinally (i.e., gas and brake). In our interface design, we use OpenPilot to control the lateral movement of the vehicle and use a simple PID controller to control the longitudinal movement to maintain a stable cruising speed.

**Control interruption mechanism modification.** Due to the overhead of the frame rendering and sending, the simulation speed cannot satisfy the real time execution requirement of the control loop, which operates at 100 Hz. Thus, without loss of functional correctness, we disable the timer interrupt in the original control loop and directly invoke 5 control iterations per frame since OpenPilot’s control loop is 5× faster than the camera frame rate (20 Hz). To match the simulation speed with the control frequency, we apply the steering angle decision of each control iteration to the LGSVL vehicle for a simulation duration of 0.01 seconds.





Figure 15: Large images of the driver's view images in Fig. 7, which correspond to the driver's view 2.5 sec (average driver reaction time [41]) before the attack succeeds under different stealthiness levels in our real world trace based attack effectiveness evaluation in §5.1. The inset figures are the zoomed-in views of the malicious road patches.



(a) Driver's view 2.5 sec before the attack succeeds in the highway scenario.



(b) Driver's view 2.5 sec before the attack succeeds in the local road scenario.

Figure 16: Large images of the driver's view images in Fig. 12, which corresponds to the driver's view 2.5 sec (average driver reaction time) before the attack succeeds in the simulation for (a) the highway scenario, and (b) the local road scenario in the end-to-end safety consequence evaluation in §6. The inset figures are the zoomed-in views of the malicious road patches.